SITE CHARACTERISATION FOR THE IUCAA TELESCOPE

H.K.Das[1] , S.M.Menon, A.Paranjpye and S.N.Tandon
IUCAA, Post Bag 4, Ganeshkhind, Pune 411 007, India

Abstract.

We present the report on characterisation of the site for IUCAA telescope, which was conducted during October '96 to April '97. The main points highlighted are the results on: seeing, contribution of atmospheric turbulence near the surface to seeing , extinction and sky brightness, cloud coverage and surface weather data. In addition the key design features of the instruments developed for these observations are presented.

Key words: Seeing, Correlation, Extinction, Sky brightness.

1. Introduction.

The Inter University Center for Astronomy and Astrophysics has chosen a site for its two metre optical telescope on a hill located at Latitude of 19°5′ N and Longitude of 73°40′ E; the height of the peak is 1005 metres. In order to optimize the telescope parameters and the scientific programmes (and the corresponding instruments), it is necessary that the parameters of the site are known and are used for selecting the programmes. With this in view, an exercise was undertaken to characterise the site for its important parameters. To help objectivity and ease of data collection it was decided to use, as far as possible, opto-electronic sensors for observations. For the purpose of these observations the following instruments were developed : differential image motion monitors for the measurements on seeing, microthermograph for estimating the contribution of the ground layer to seeing, CCD camera for extinction and sky-brightness measurements, photometer for sky-brightness measurements, and wide angle CCD camera for detecting clouds. In addition to these instruments, a standard auto-recording weather station was used. In the following sections a brief description of these instruments is presented in addition to the results obtained on

[1]email: hkdas@iucaa.ernet.in

the site.

2. Seeing.

2.1 Measurements of seeing.

Description of the monitor.

The seeing monitor is designed keeping in view the principle of a differential image motion monitor (DIMM). The DIMM principle is to produce twin images of a star with the same telescope via two entrance pupil separated by a fixed distance. The advantage of this differential method is that it eliminates tracking errors; (see Bisht *et al.* 1990)

Our system consists of two arms (Fig.1) which are separated by one metre. Each arm supports a f/12 lens which is fifteen centimetres in diameter. Fig.1 explains how the two images of a star are formed in the focal plane where an ST6 CCD camera is mounted. The total weight of the monitor is about seventy kgs, and it is mounted such that the lenses are at a height of about two metres above the ground.

Principle and theory.

A series of fifty frames, each with an exposure time of ten milliseconds are taken and stored in a laptop PC. The separation between the images of the star is about twenty pixels.

Next, the centroids for each star image of each frame is calculated. The variance of the separation between the two centroids in the longitudinal (parallel to direction of separation of the two lenses) and transverse (perpendicular to direction of separation of the two lenses) components respectively are given by (Sarazin and Roddier, 1990),

$$\sigma_l{}^2 = [1 - 0.541 S^{-1/3}]\sigma^2, \tag{1}$$

$$\sigma_t{}^2 = [1 - 0.811 S^{-1/3}]\sigma^2, \tag{2}$$

where,

$$\sigma^2 = 0.358(\lambda/r_o)^{5/3}(\lambda/D)^{1/3}, \tag{3}$$

which is defined as the variance of the image position through a single aperture of diameter D; r_o is the Fried parameter for the zenith angle of measurement. The value of S for our monitor is 6.67 which is defined as the ratio between the separation of the two lenses to their diameter. σ_l and σ_t are calculated from the stored frames, and

using Eqn.3 in Eqn.1 and Eqn.2 we can get two values of r_o. The FWHM (in radians) for zenith is,

$$FWHM = 0.98(\lambda/r_o)(\cos\gamma)^{3/5}, \tag{4}$$

where γ is the zenith distance of the star on which measurement is made; (we made all our measurements on the pole star).

Results.

We present our results in Table 1. The histograms in Fig.2 and Fig.3 are the results of our measurement in December '96 and April '97, which have the best and the worst average seeing respectively.

Statistical errors.

It is important to know the contributions of errors in the measurements of σ_l and σ_t. To estimate the accuracy of the centroid measurement, we simulated the images of seeing monitor with the images of two pinholes in the laboratory; the separation and size of the images on the CCD were similar to the one in the monitor.

Mainly two types of variation contribute significantly to the resultant errors in the measurements, they are:

(a) Variations due to photoelectron statistics, over a set of frames for fixed position of the images; it would be a function of the image brightness and we denote the corresponding variance by by $\sigma^2(I)$. (The contribution from the background noise is negligible; and the following calculation is inclusive of all background contributions, if any.)

(b) Variations, due to intrapixel nonuniformities as the centroids of the images move across the pixels; we denote the corresponding variance as $\sigma^2(p)$.

Therefore,

$$\sigma^2_{total} = \sigma(p)^2 + \sigma(I)^2 \tag{5}$$

From the measurements made in the laboratory we find that

(1) σ_{total} is nearly equal for longitudinal and transverse components, and

(2) σ_{total} increases with decreasing intensity of the images;

their values being 0.12 arc sec for an intensity corresponding to images under clear sky; and being 0.18 arc sec for intensity which is less by a factor of four. These errors are quite small as compared to σ_l and σ_t.

2.2 Measurement of the contribution of atmospheric turbulence near the surface to seeing.

Principle and theory.

The results obtained with the seeing monitor have been discussed in the previous sub section; they give an estimate of the seeing at a height of two metres. To find out if we would get better results if we increased the height by another ten metres (say), we performed measurements of micro-thermal variations to estimate contribution of the ground layer to the seeing.

One pair of micro thermal sensors (made with 20 micron diameter tungsten wire) separated by a distance of one metre is mounted at a height of two metres above the ground, and, another pair similarly separated by one metre is mounted at a height of eight metres above the ground.

A data-logger records the mean of the magnitude of temperature difference (i.e $\mid \triangle T \mid$) for each pair of sensors. The frequency band of measurements is 0.1 Hz to 10 Hz; this is adequate because the typical wind speeds are a few metres/sec, which leads to a time scale greater than 0.1 sec over one metre separation. The signal from the sensors are stored in volts which is later converted into corresponding temperature and seeing values.

The measurements are used to estimate the value of ${C_T}^2(h)$ which is the temperature structure constant. The refractive index structure constant ${C_N}^2(h)$ can be obtained as, (Marks *et al.* 1996)

$$ {C_N}^2(h) = (\frac{80 \times 10^{-6} \times P(h)}{T^2(h)})^2 C_T^2(h), \tag{6} $$

where, P(h) is the pressure in millibars and T(h) is the temperature in $^\circ K$ across any height h.

The corresponding FWHM (in radians) can be obtained from, (Marks *et al.* 1996)

$$ FWHM = 5.25\lambda^{-1/5}(\int_0^H C_N^2(h)dh)^{3/5} \tag{7} $$

Relation of micro thermal measurement to seeing .

Assuming the temperature fluctuation to be sinusoidal we can write,

$$ C_T^2 \approx 2(< \mid \triangle T \mid >)^2 \tag{8} $$

If we assume that the structure constant C_T is uniform across ten metre height and all the seeing is over the ten metre height, then for λ=5000 $\dot{A}$, H=10 metre, P at a location 1000 metre above sea level and $T = 20°C$ we get from the above Eqns.

$$FWHM = 6.3\ (< \mid \triangle T \mid >)^{1.2} \quad arc\ sec. \tag{9}$$

Results.

The results are presented graphically in Fig.4 and Fig.5 for both day and night data records. The conversion to corresponding values of seeing in arc seconds is done assuming a ten metre air column with uniform C_T^2.

It is seen that the bottom sensors show somewhat larger fluctuation, but even for the C_T^2 corresponding to these, the calculated contribution to seeing is less than 0.5 arc sec. We thus conclude that most of the observed seeing is arising from heights beyond ten metres.

2.3 Correlation of weather parameters with seeing

To see whether any correlation exists between seeing and weather parameters, the two variables are plotted along the two axes of a two dimensional graph. Existence of a consistent pattern between the two variables indicates presence of correlation. We plotted the difference between the maximum and the minimum wind speed (which is a measure of the degree of gustiness), average wind speed, and the difference between maximum and minimum air temperature (which is a measure of the degree of temperature fluctuation) over a period of half an hour, against the mean seeing values over this period to examine the existence of any relation; these are shown in Figs.6 to 8.

From Fig.6 we see that as the gustiness increases there is a corresponding increase in the seeing value as well; from Fig.7 we see that the seeing value also increases with an increase in the average speed. Further, this increase in seeing is comparable to the spread in seeing at any value of the wind speed parameter. On the other hand Fig.8 shows that as the temperature fluctuation increases, the seeing does not change significantly.

2.4 Noise due to shaking of the Seeing Monitor.

The correlation between the wind speed and seeing could be due to shaking of the instrument by wind forces. To find out what is the degree of contribution to observed seeing values due to shaking of the monitor, we did the following:

For sets of fifty frames, the ratio:

$$\frac{\text{(standard deviation of the separation between the images)}}{\text{(standard deviation of the position of one of the images, after subtracting a uniform drift along a straight line)}}$$

was plotted against the measured seeing.

Any shake will reduce this ratio, because the positions of the individual images will change more as compared to the separation between them; this is illustrated by Figs.9 and 10 which were obtained by purposely tapping the monitor in both transverse/longitudinal direction while recording the frames. It is seen that in these observations the ratio (plotted on the ordinate) is in range 0.1 to 0.2. On the other hand the Figs.11 and 12 corresponding to the normal observation show that the ratio (plotted on the ordinate) has a spread in range 0.1 to >1. From this comparison we conclude that for seeing values < 2 arc sec, shaking of the instrument due to wind is not a major source of error.

3. Extinction and Sky Brightness.

3.1 Extinction measurements.

To measure the atmospheric extinction, standard photometric stars, given in Table 2, were used. A 50mm, f/1.8 Nikon lens mounted on a ST6 CCD camera was used for the measurements; the sky cover per pixel (23 μm X 27 μm) is 91.2 X 107 Sq. arc sec. Johnson B,V filters mounted in a lens cap were placed before the lens. The diameter of the filters is 22mm, thus the effective f-ratio of the lens was equal to 2.27. The diameter of the filter was chosen to ensure that with the full aperture of the lens there was no vignetting.

The CCD camera is mounted on a medium heavy duty camera stand. A guide scope (X 7, magnification) with a cross hair was attached to the CCD camera for sighting the stars. A laptop computer was used for recording the CCD frames.

To get the estimates of extinction two stars one at zenith distance $< 10°$ (air mass ≈ 1) and one at zenith distance $> 50°$ and $< 60°$ (air mass ≈ 2) were observed within a span of several minutes. The stars were also followed for air mass in the range 1 to 2.

Using the same data the sky brightness (in B and V band) was also estimated, which was used to calibrate the night sky photometer data.

Results

The extinction range in B band varies from 0.26 to 0.74 mag/air mass; and from 0.14 to 0.38 mag/air mass in the V band. However, the mean extinction in B and V band are 0.46 and 0.28 mag/air mass respectively.

3.2 Sky Brightness.

The sky brightness was measured with a simple photometer in which a photodiode (3.9 mm X 4.6 mm) is exposed to the sky in a solid angle (about 0.65 steradian) defined by a cylindrical baffle. The photodiode is covered with a filter to select V, B, or R band. It was calibrated for V and B band by comparing with the CCD camera described in the preceding sub-section. The calibration for the R band was obtained by observing moon through V-band and R-band within a short interval. Based on the calibration for the V-band the sensitivity for the R-band is then derived using a V-R colour index of 0.8 mag for moon (Harris in *Planets and Satellites, 1961*) and a differential extinction of ($\triangle$V - $\triangle$R) of 0.2 mag.

Results.

The sky brightness in all B, V, and R are presented as histograms in Figs.13, 14 and 15. Typically it is 22 $mag/(arcsec)^2$ in B-band, 21 $mag/(arcsec)^2$ in V-band, and 19.4 $mag/(arcsec)^2$ in R-band. Their mean values at three different periods of the night are presented in Table 3.

4. Cloud cover.

4.1 Visual observations.

To have an approximate idea as to how many photometric and how many spectroscopic nights can we get at our site, we made a visual cloud record of the sky for over a period of six months.

To do so we divided the entire sky into eight division, each division corresponding

to a count of one octant. Thus for one time observation we get a maximum count of eight octants for the entire sky. We noted the sky condition four times every night, thus the total sky count per night corresponds to a maximum of thirty two octants.

We then applied the following criterion to draw a conclusion:

1. If 32 octant count corresponds to clear sky, then the sky is both photometric and spectroscopic.

2. If more than 16 octant count of the sky corresponds to regions covered with clouds, then that night is rejected.

3. If more than 8 octant count of the sky corresponds to regions covered with thick clouds then also the night is rejected.

4. Otherwise the night is only spectroscopic.

As shown in Table 4 about 50 % of the nights are thus photometric and 80 % of the nights are spectroscopic during the period.

4.2 Cloud detection with a CCD camera.

In section 4.1 we have described the results from visual recordings of the cloud cover. In order to develop an objective photoelectric method of recording clouds, which would be more objective and possibly more sensitive, we made observations with a wide angle CCD camera.

Method of observation.

Images of the sky are taken in four directions (North,East,South and West) in a sequence. This was done with a wide angle CCD camera, which consists of a f/1.8, 6.5 mm wide angle (60° FOV) lens mounted on a ST6 CCD camera; the elevation of the camera axis was kept at 55° whereas the azimuth angle was kept at 0 °, 90°, 180° and 270° respectively; these four exposures cover about one half of the sky. In order to minimise the effects of variations in the clear air extinction, a filter was used to restrict the bandpass to $\lambda \geq 5500\dot{A}$; the CCD characteristics give an upper wavelength cutoff $\approx 8500\dot{A}$.

For each direction such images with fifteen seconds exposure time were taken four times every night with about two hours interval. With fifteen seconds exposure we could detect fourth magnitude stars with about 10% photometric accuracy. The

images in a particular direction at a particular time, correspond to a particular star field. To get the same star fields on several nights, the images on any night were taken at times which were four minutes prior to the previous night's observation time. This procedure gave images of the same fields over a period of about fifteeen days.

Analysis.

Out of the several frames of the same star field, one frame which showed no sign of clouds on inspection on the computer display was chosen as the reference frame, and about seventeen to twenty stars were identified in it. The total flux (across appropiate aperture) of each chosen star in the frame was obtained by using IRAF (Digiphotx). Similarly, the total flux for these stars was obtained in all the other frames.

Next we obtain the flux ratios of a particular frame to reference frame corresponding to all the chosen stars. This was done for all the frames of the set corresponding to the same field. To explain further :

Suppose we define F_d(i,n) as the flux of the i^{th} star in the n^{th} frame. Let the r^{th} frame be chosen as the reference frame, the ratios F_d(i,n)/F_d(i,r) are calculated for all the stars (i's) and all the frames (n's). The mean and standard deviation of these ratios are then found. A mean which is significantly less than one (say < 0.8) and/or a large standard deviation indicates presence of clouds.

In order to guard against errors due to variable stars, cosmic-ray hits, or other single shot noises, stars which showed large standard deviation in flux ratios over the set of frames were rejected; a total of twelve stars from thirty two fields (each field has about fifteen frames) were rejected on this basis.

We present our data for two months (Nov. '96 and Feb. '97) in Fig.16. The means and the standard deviations of the flux ratios are plotted in these figures; each category of the night (as per the criteria of Section 4.1) is shown by a different symbol.

These figures show that the photometric nights tend to show a higher value of the mean flux ratio as compared to the spectroscopic night, but the standard deviations are similar for the two kinds of nights. The means have a much larger scatter for the photometric nights in February as compared to the nights in November - this indicates that the CCD camera is able to detect the increased extinction due to uniform clouds or fog. Some of the data points show clear inconsistencies between the CCD frames and the visual records - some of these could be due to the inability of the human observers to record uniform cloud/fog, but others suggest wrong record of clouds by the observers.

5. Surface Weather Data

A weather station was installed at the site to measure some of the parameters that characterize the surface weather. It consists of a three metre tall tower on which sensors are mounted. They measure the following parameters :

1. Air temperature,
2. Wind speed, and
3. Wind direction

The data collected over a period of one year has been divided into three different seasons, monsoon, winter and summer. They are presented in the form of histograms in Figs. 17 to 25. Our wind direction measurement sensor has been calibrated where 0° corresponds to North, 90° to East, 180° to South, and, 270° to West.

It is interesting to note that though in winter the wind direction is mostly easterly, in summer and monsoon it is mostly westerly; but the trend is always east $\rightleftharpoons$ west. The maximum wind speed most of the time ranges between 2 to 10 m/sec, and average wind speed ranges between 1 and 5 m/sec.

6. Conclusion.

The following main characteristics have been observed for the site: the mean seeing value ($\approx$ 1.5 arc sec. during peak observation seasons) is comparable with other good Indian sites. There is however some difference between the values obtained from the two components of image motion; wind speed and the finite outer scale length will effect the correlation between the two apertures, and could lead to this difference.

Contribution of atmospheric turbulence near the surface (across ten metre air column) to seeing is also small ($<$ 0.5 arc sec.). Most of the seeing is therefore originating from regions beyond ten metre height.

The mean atmospheric extinction in B and V band are 0.46 and 0.28 mag/air mass. Sky brightness has values of 21.82, 20.89 and 19.46 $mag/(arcsec)^2$ in all B, V, and R-band.

Manual observations of the cloud cover shows that in the months November '96 to April '97, 50% of the nights are photometric and 80% of the nights are spectroscopic. Comparison of the manual observations and the pictures taken with a wide angle CCD

camera show that the CCD camera is more efficient in detecting uniform clouds/fog of optical thickness ≥ 0.2.

Acknowledgement.

We are thankful to our project students Rishikesh Ghare for developing the software to calculate the centroids of the star images, and to Putlibai Nongthombam for developing the electronic circuit board to record data from micro thermal sensors.

We are thankful to our colleagues Somak Raychaudhury for hearty discussions while analysing the cloud images and to Vilas Mestry for rendering timely help in the electronic laboratory as and when required.

We are indebt to Sunil Nayar, Abhay Kohok, Anantwal Maruti, D.K.Dhumal, Santosh Gore, Arvind Jagtap, Pradip Dhande and Ashok Gopale for carrying out the observation at the site.

Table 1. Percentage of seeing values (longitudinal component) within a particular range and their median values for that month.

Month	s<1″	1″<s<1.5″	1.5″<s<2″	Median
Nov.'96	3%	54%	38%	1.4″
Dec.'96	14%	42%	27%	1.4″
Jan.'97	9%	36%	33%	1.6″
Feb.'97	5%	48%	32%	1.5″
Mar.'97	1%	42%	40%	1.8″
Apr.'97	0.4%	19%	35%	2″

Table 2. Standard photometric stars used to measure extinction.

Star	RA	DEC	V	B - V	Sp. Type
	h m s	d m s			
π^3 Ori = HR 1543	04 49 42.3	06 57 25	3.19	+0.46	F6
π^4 Ori = HR 1552	04 51 04.4	05 36 03	3.68	- 0.16	B2
γ Gem = HR 2421	06 37 34.1	16 24 06	1.92	0.00	A1
α Leo = HR 3982	10 08 14.3	11 58 46	1.35	- 0.11	B7
ρ Leo = HR 4133	10 32 40.8	9 19 10	3.85	- 0.14	B1
β Leo = HR 4534	11 48 55.9	14 35 10	2.14	+0.08	A3
τ Boo = HR 5185	13 47 08.6	17 28 09	4.50	+0.48	F7
η Boo = HR 5235	13 54 33.9	18 24 37	2.68	+0.58	G0
γ Lyr = HR 7178	18 58 51.0	32 41 10	3.24	-0.05	B9

Table 3. Mean sky brightness (in $mag/(arc\ sec)^2$) at three different periods of the night, measured between February - May 1997.

Band	21:00 - 00:00 hrs.	00:00 - 02:00 hrs.	02:00 - 05:00 hrs.
B	21.80	21.82	21.94
V	20.76	20.89	20.97
R	19.29	19.46	19.54

Table 4. Number of photometric and spectroscopic nights over a period of six months.

Month	No. of nights recorded	Photometric	Spectroscopic
Nov.'96	26	14	23
Dec.'96	12	4	8
Jan.'97	20	14	16
Feb.'97	21	21	21
Mar.'97	26	9	16
Apr.'97	24	5	20
Total	129	67	104

References.

1. Bisht R.S. *et al.* , 1990 *PASP* , **102**, 590.

2. Harris, Daniel L., *Planets and Satellites*, eds. Kuiper, G.P., and Middlehurst, B.M. 1961, p.303, Table 17.

3. Marks, R.D., Vermin, J., Azouit, M., Briggs, J.W., Burton, M.G., Ashley, M.C.B, Manigault, J.F., 1996, *Astron. Astrophys. Suppl. Ser.* , **118**, 385 - 390.

4. Sarazin, M., Roddier, F., 1990 *Astron. Astrophys.*, **227**, 294 - 300.

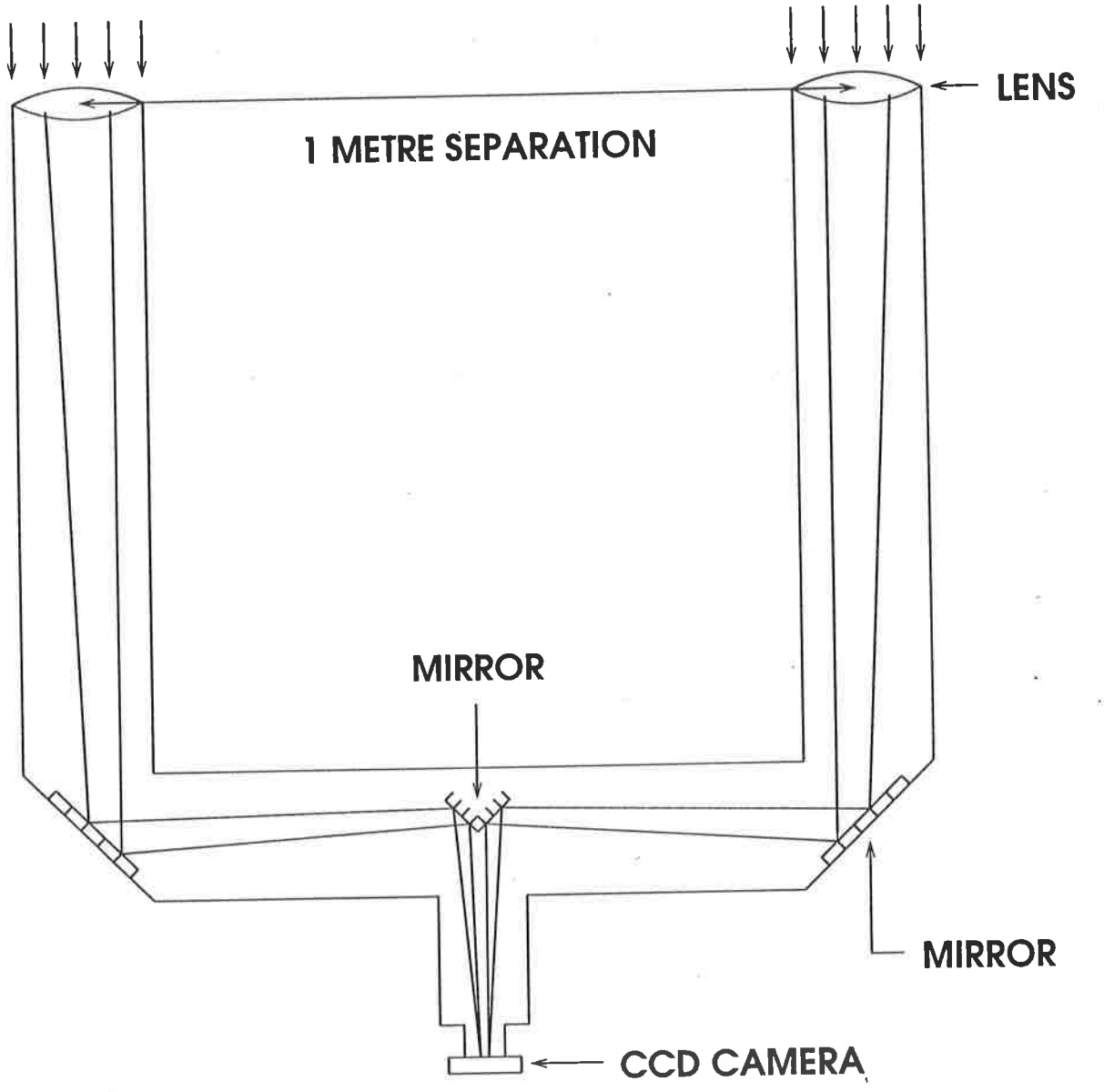

Figure 1. Ray diagram showing how two images of a star are formed by the seeing monitor.

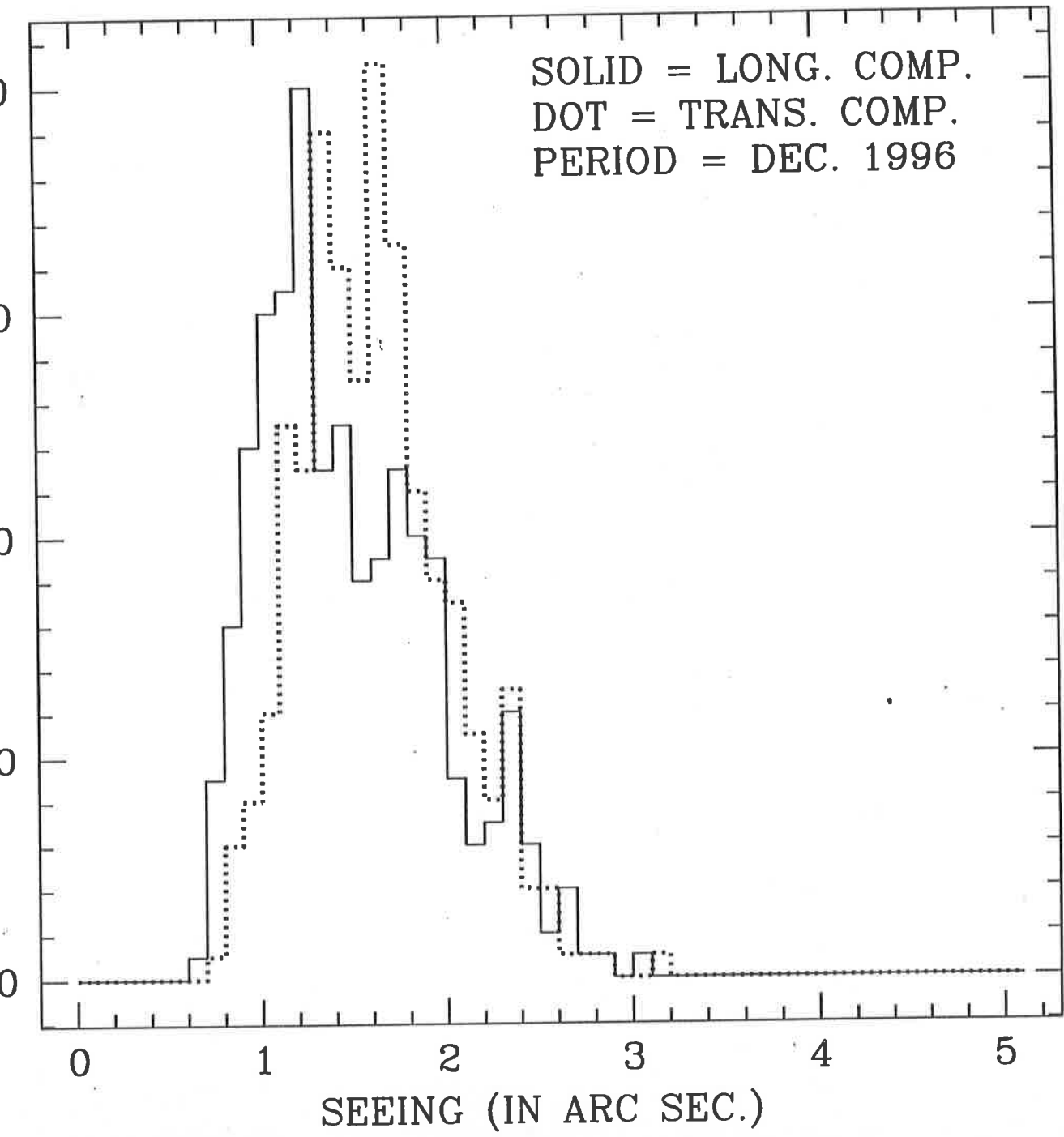

Figure 2. Histograms of the measured seeing values during December '96; the solid histogram is for the values obtained from longitudinal component of the image motion, and the dotted component corresponds to the value obtained from the transverse component.

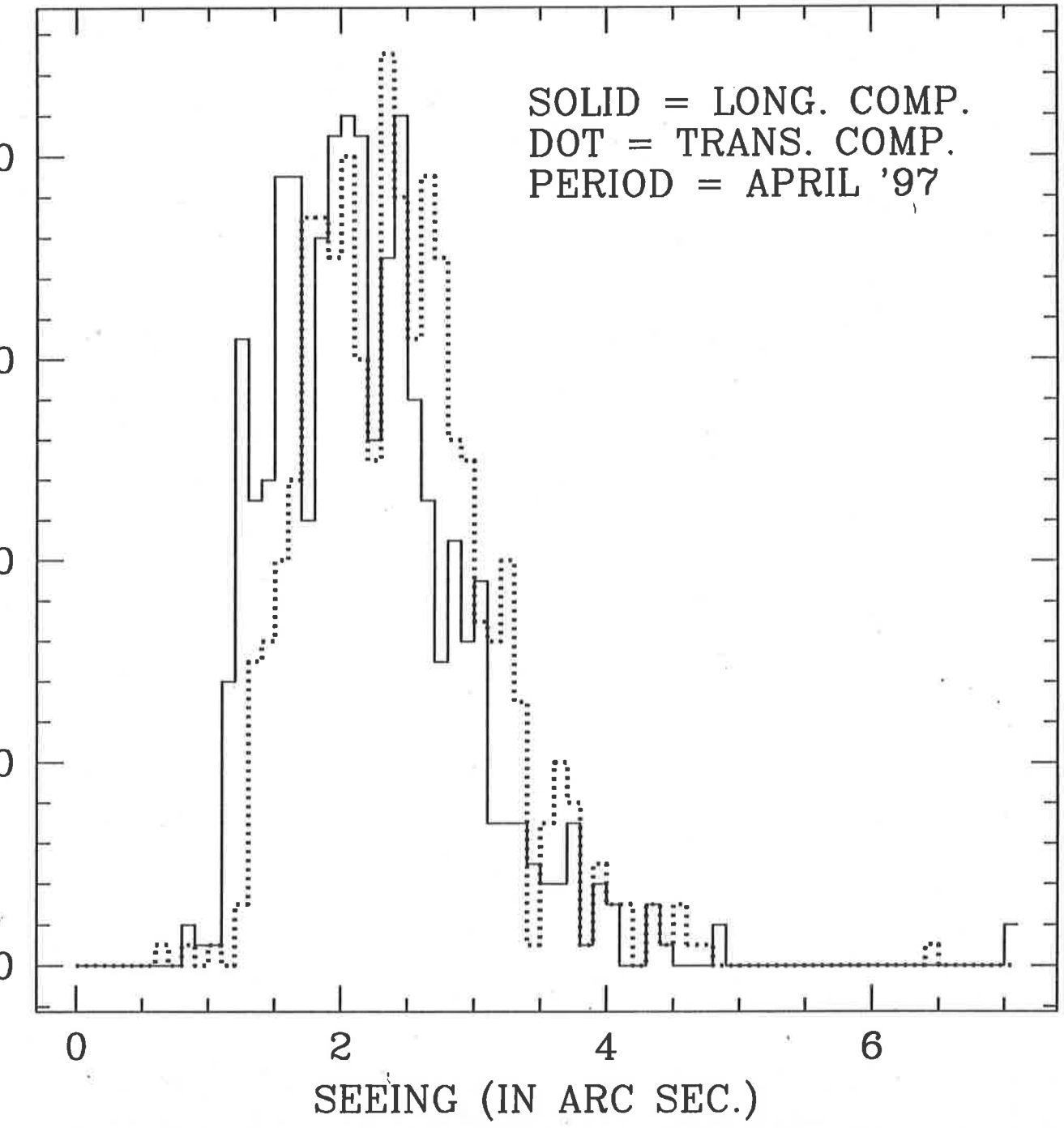

Figure 3. Histograms of the measured seeing values during April '97; the solid histogram is for the values obtained from longitudinal component of the image motion, and the dotted component corresponds to the value obtained from the transverse component.

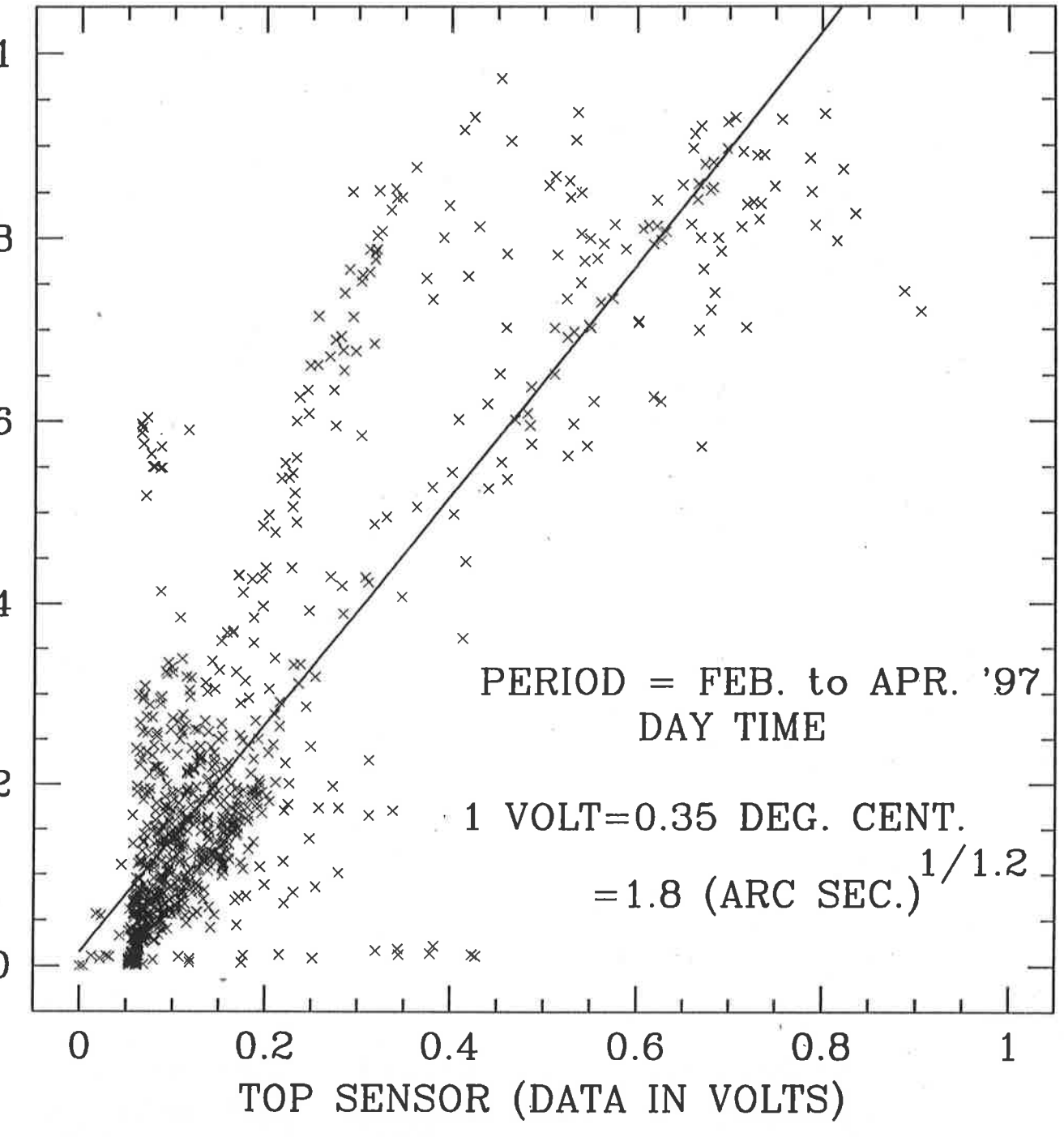

Figure 4. Micro thermal sensor data (in volts) during day for both the top and bottom sensors.

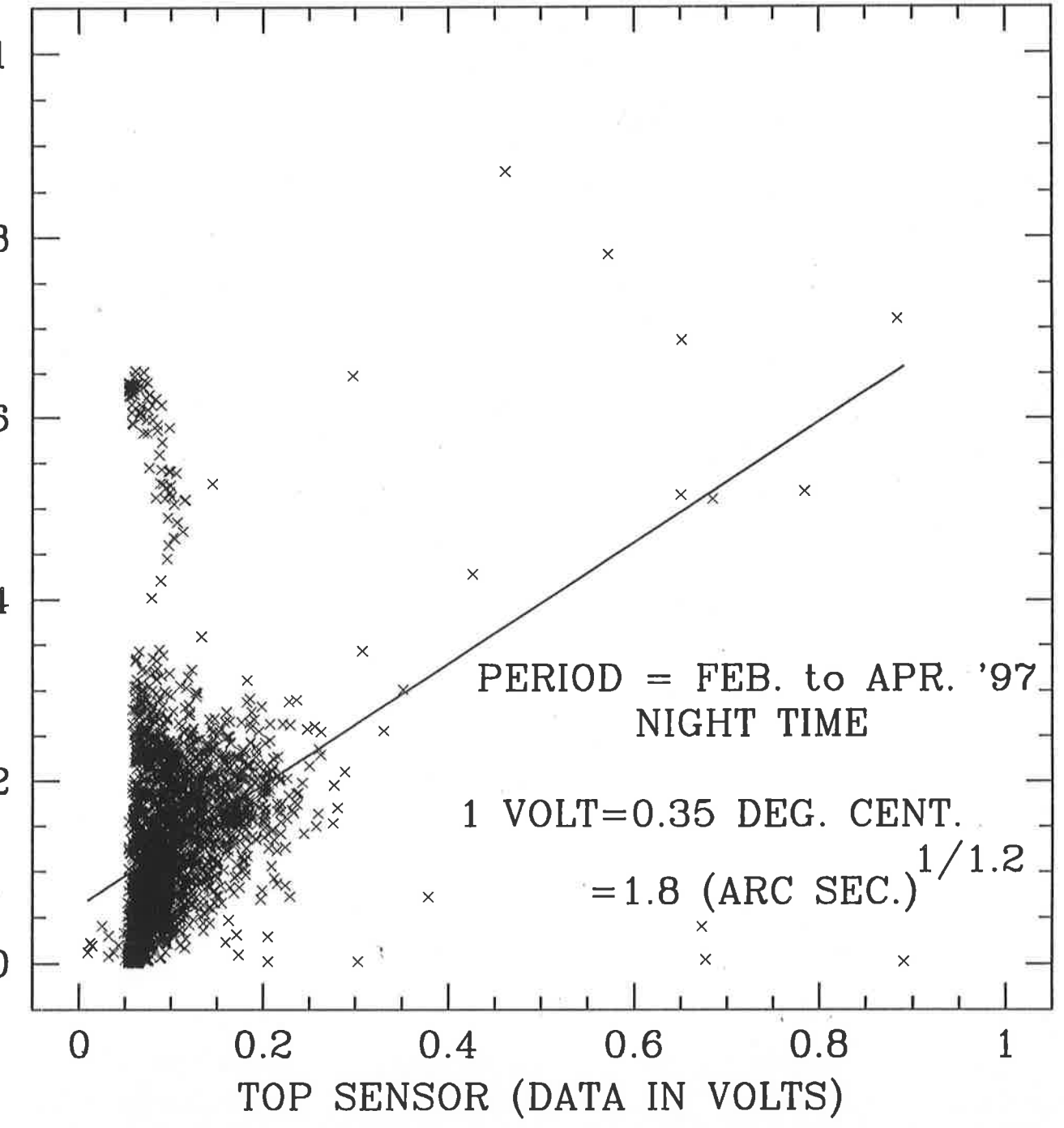

Figure 5. Micro thermal sensor data (in volts) during night for both the top and bottom sensors.

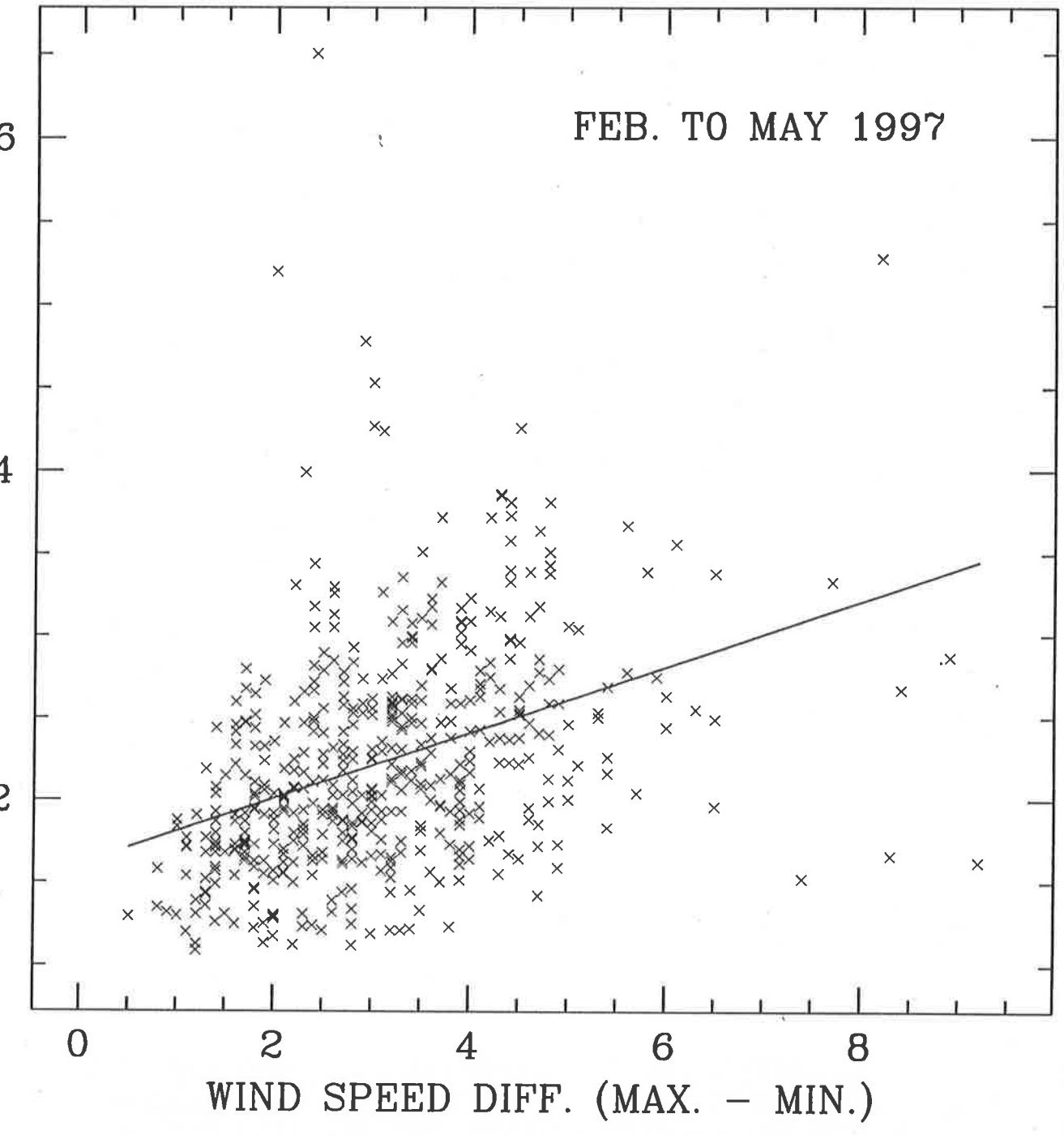

Figure 6. Correlation between the wind gustiness and the measured seeing values for one of the components - transverse component.

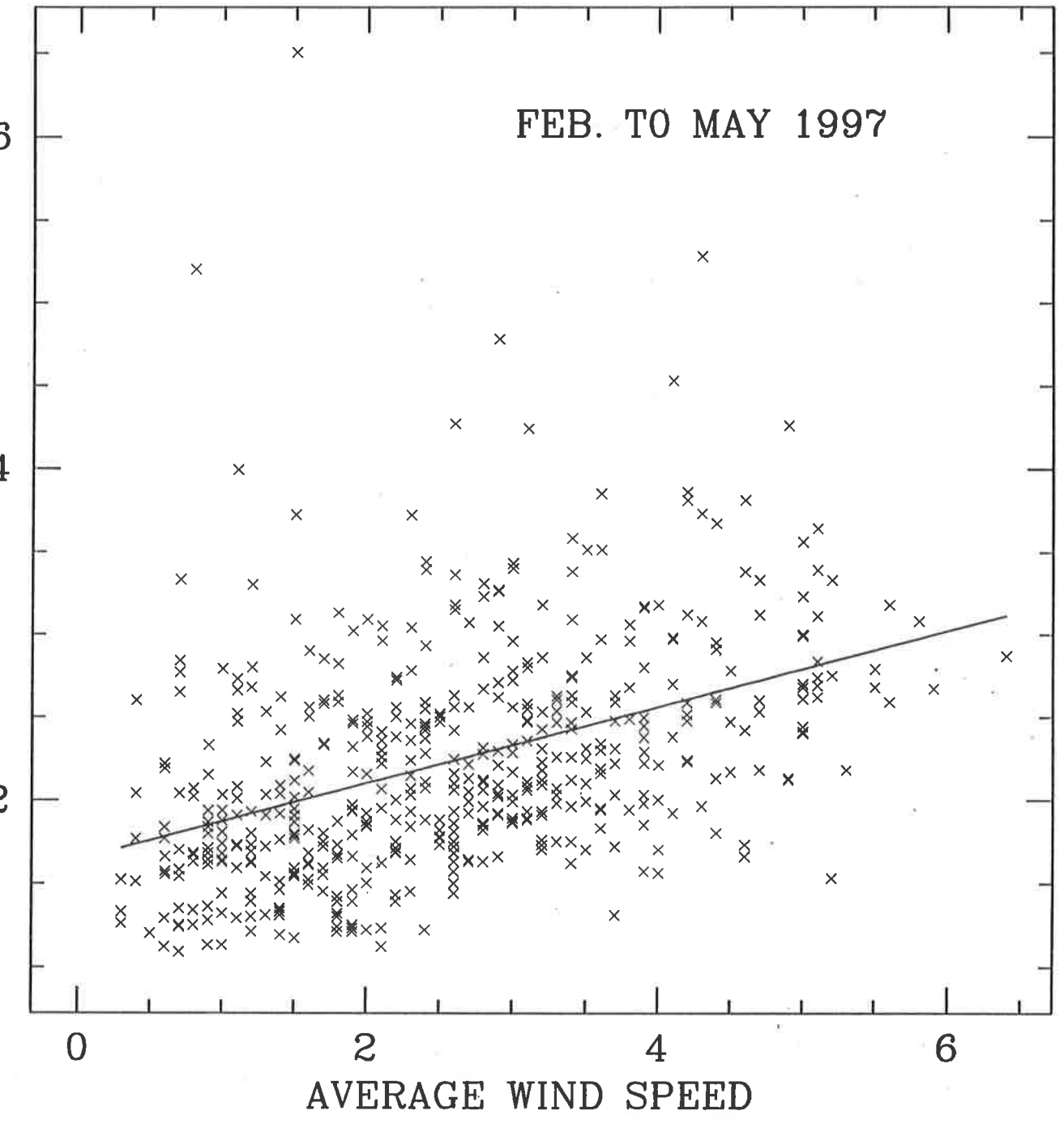

Figure 7. Correlation between the average wind speed and the measured seeing values for one of the components - transverse component.

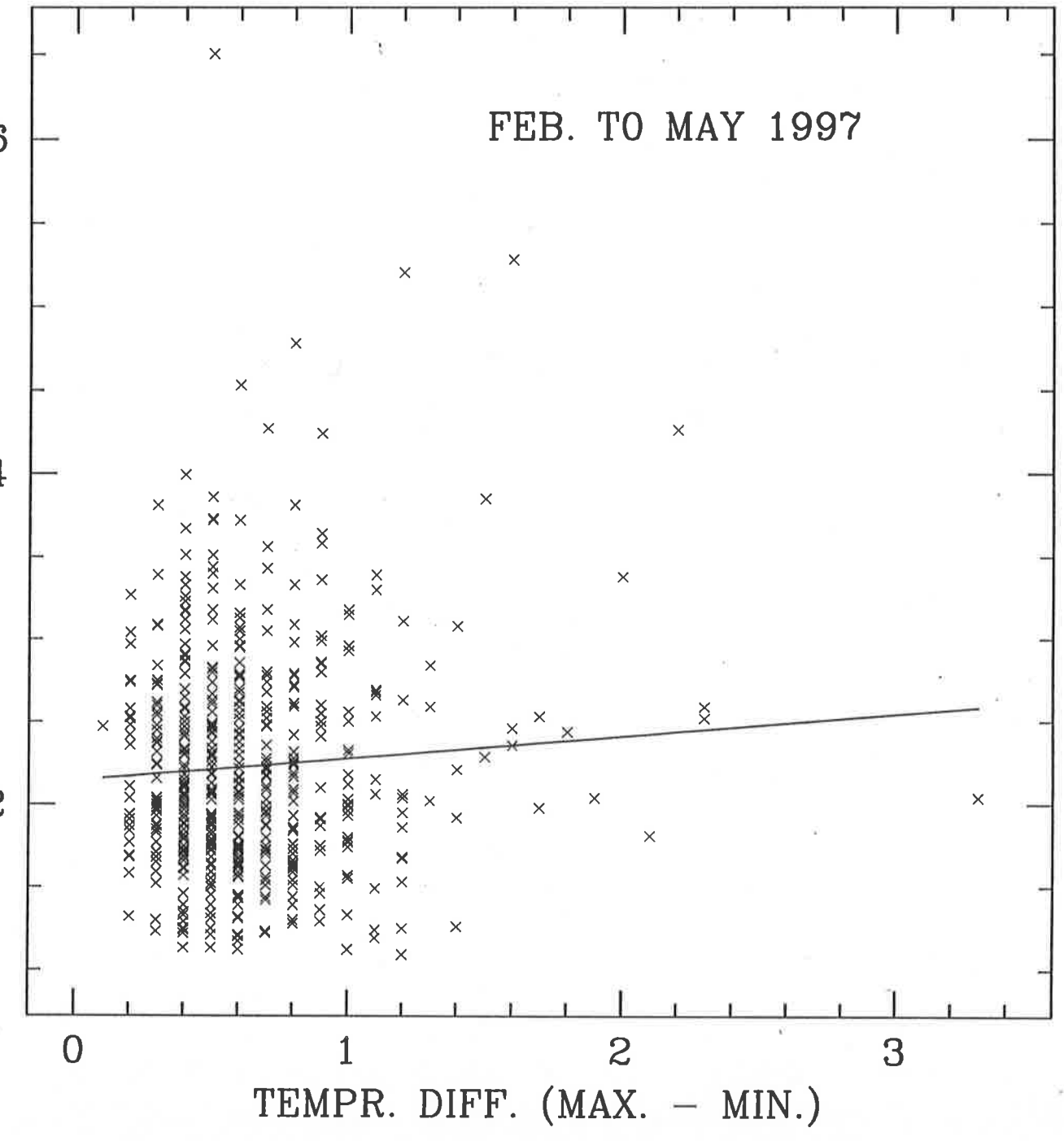

Figure 8. Correlation between the temperature fluctuation and the measured seeing values for one of the components - transverse component.

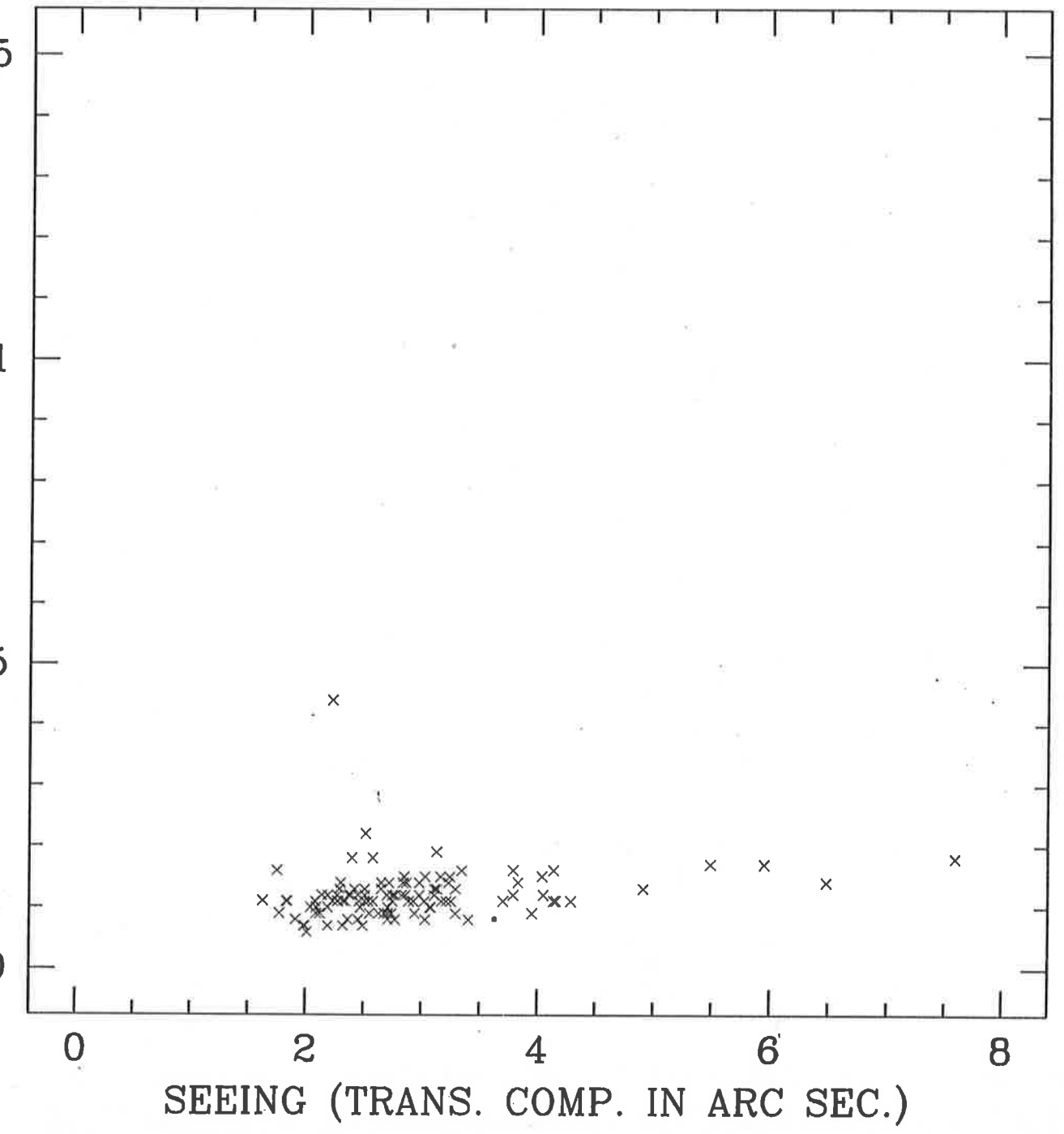

Figure 9. Ratio of the standard deviation of the separation between the two images to the standard deviation of the centroid of one of the images which were obtained while tapping the monitor in the transverse direction.

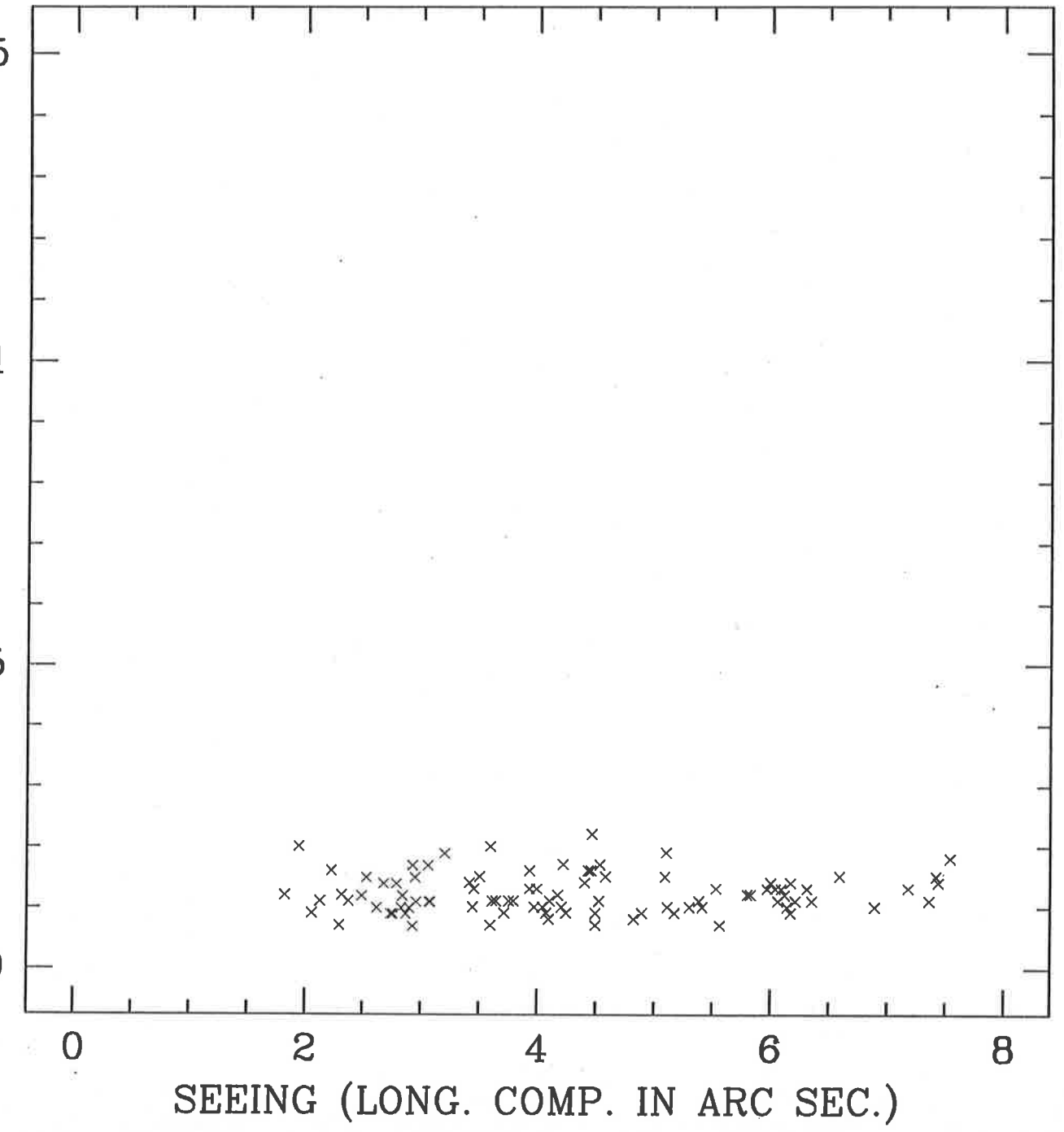

Figure10. Ratio of the standard deviation of the separation between the two images to the standard deviation of the centroid of one of the images which were obtained while tapping the monitor in the longitudinal direction.

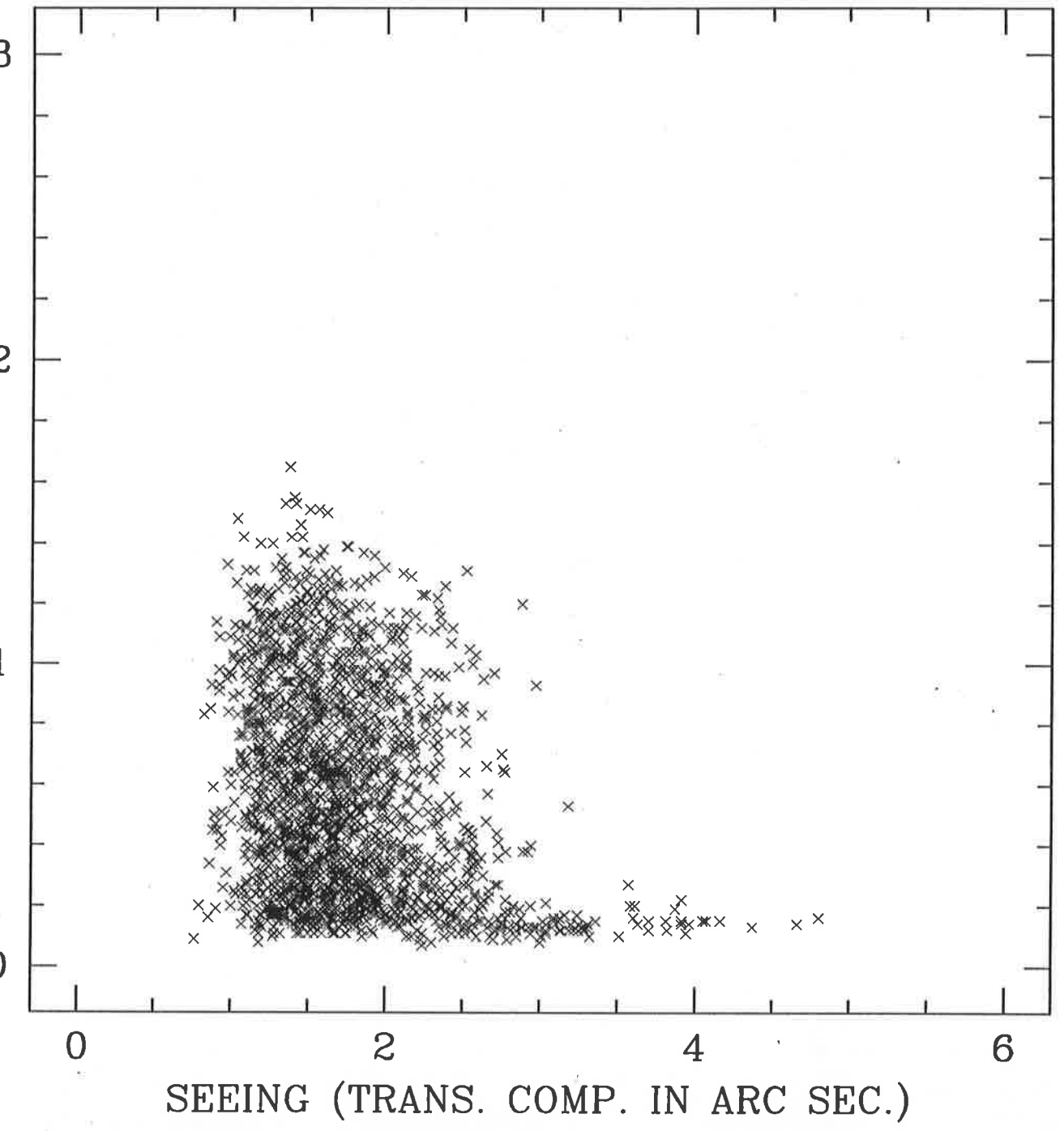

Figure 11. Ratio of the standard deviation of the separation between the two images to the standard deviation of the centroid of one of the images which were obtained corresponding to normal observation.

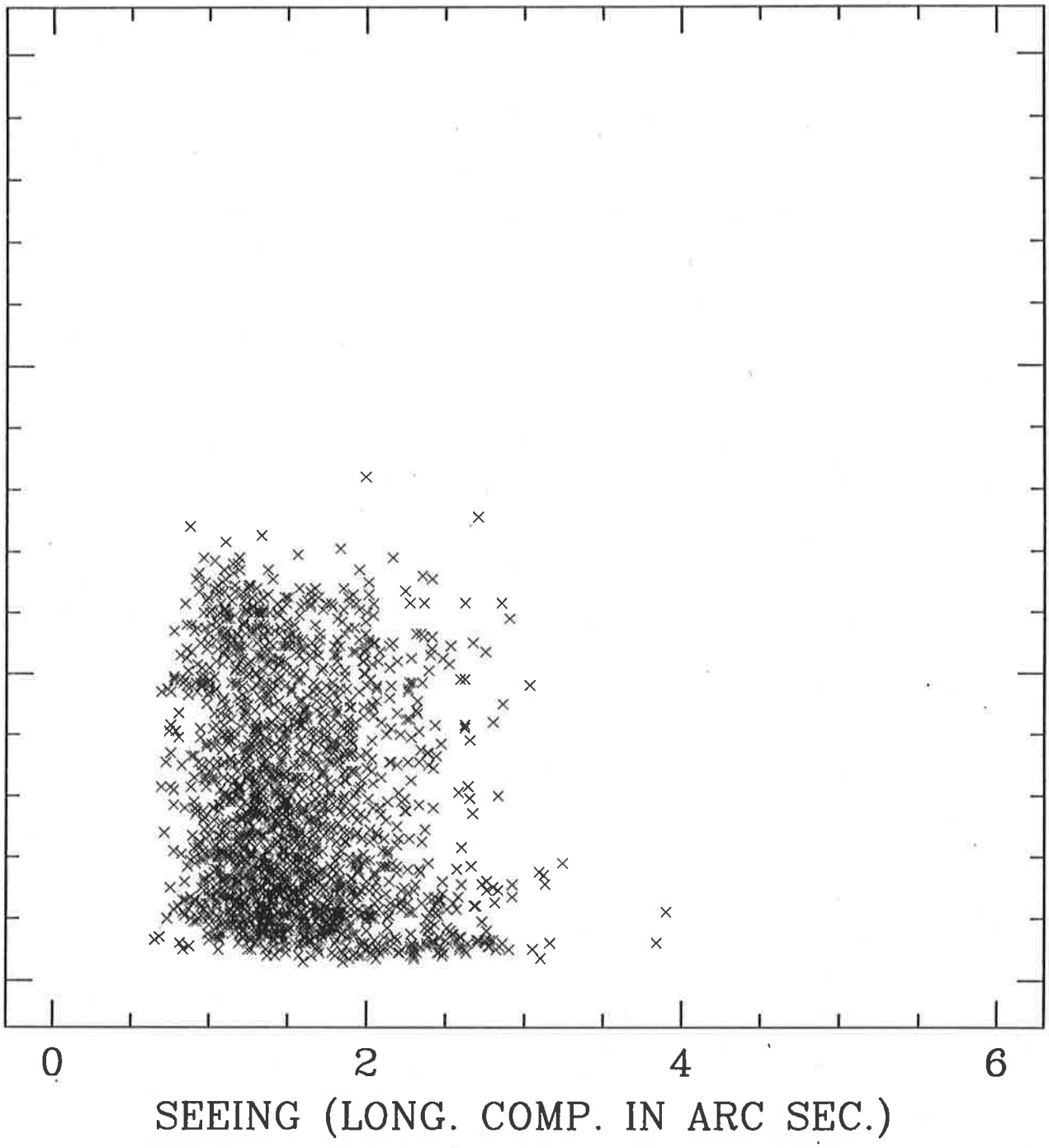

Figure 12. Ratio of the standard deviation of the separation between the two images to the standard deviation of the centroid of one of the images which were obtained corresponding to normal observation.

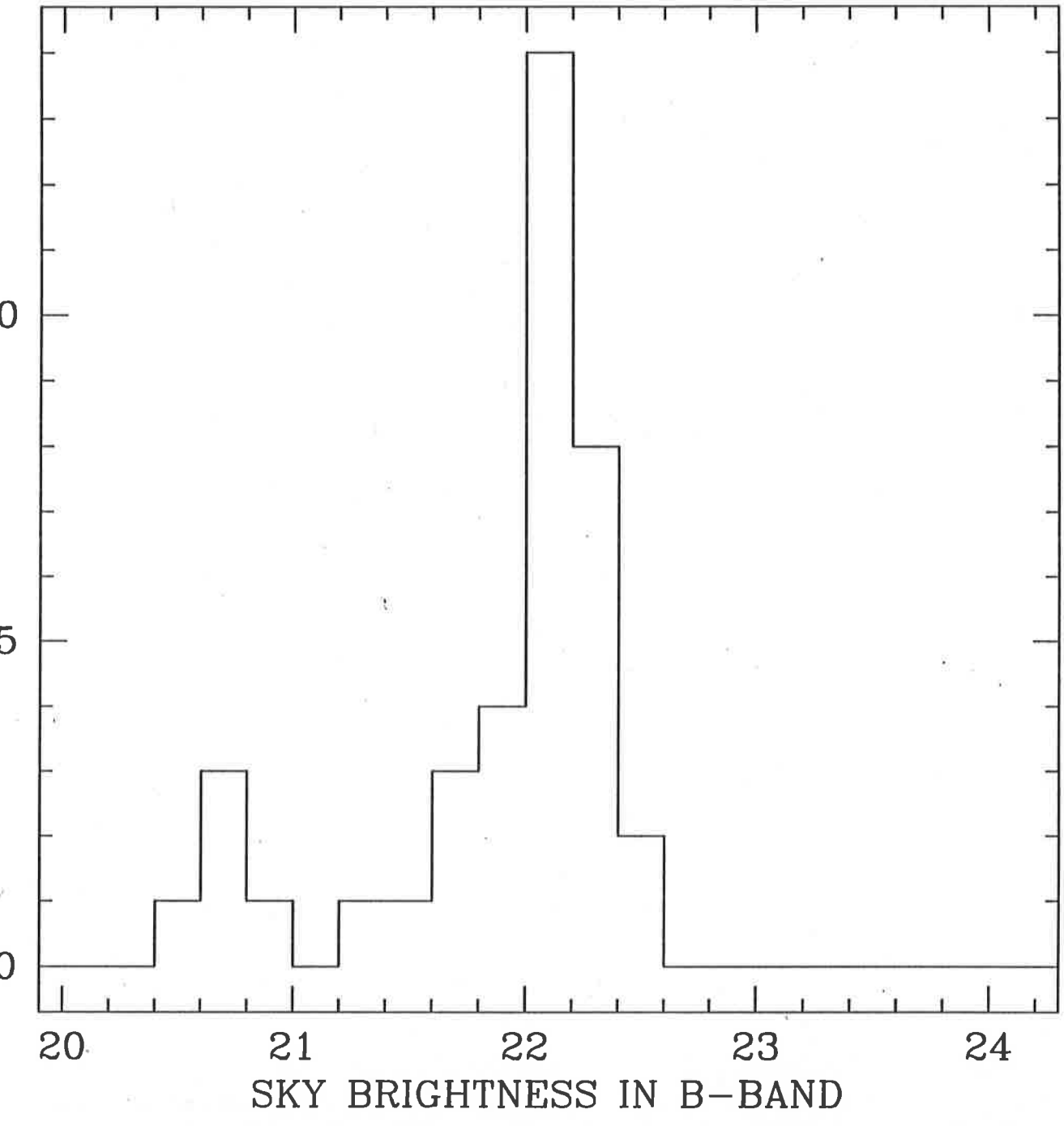

Figure 13. Histogram of the measured sky brightness ($mag/(arcsec)^2$) in B-band during February-May '97.

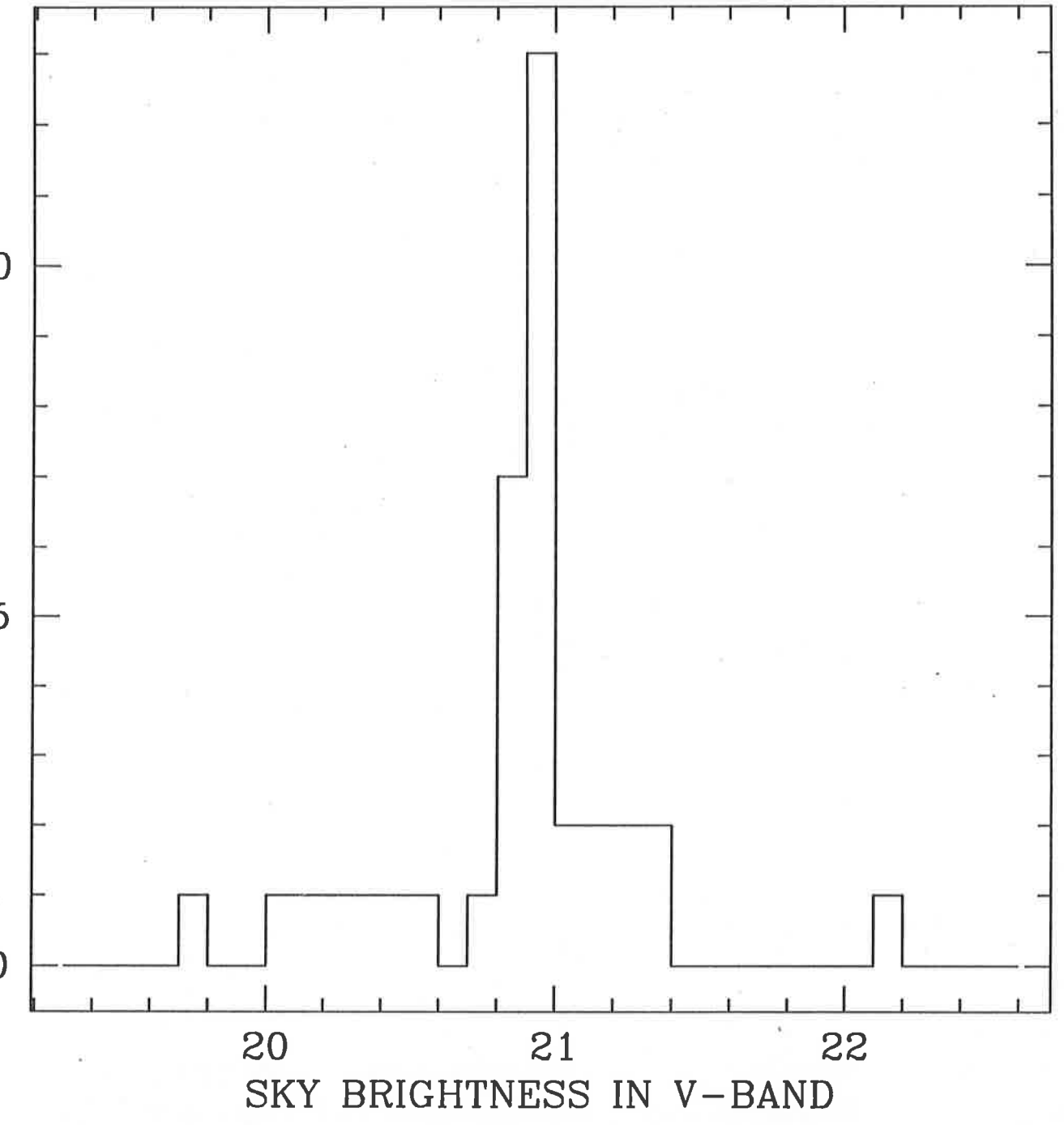

Figure 14. Histogram of the measured sky brightness ($mag/(arcsec)^2$) in V-band during February-May '97.

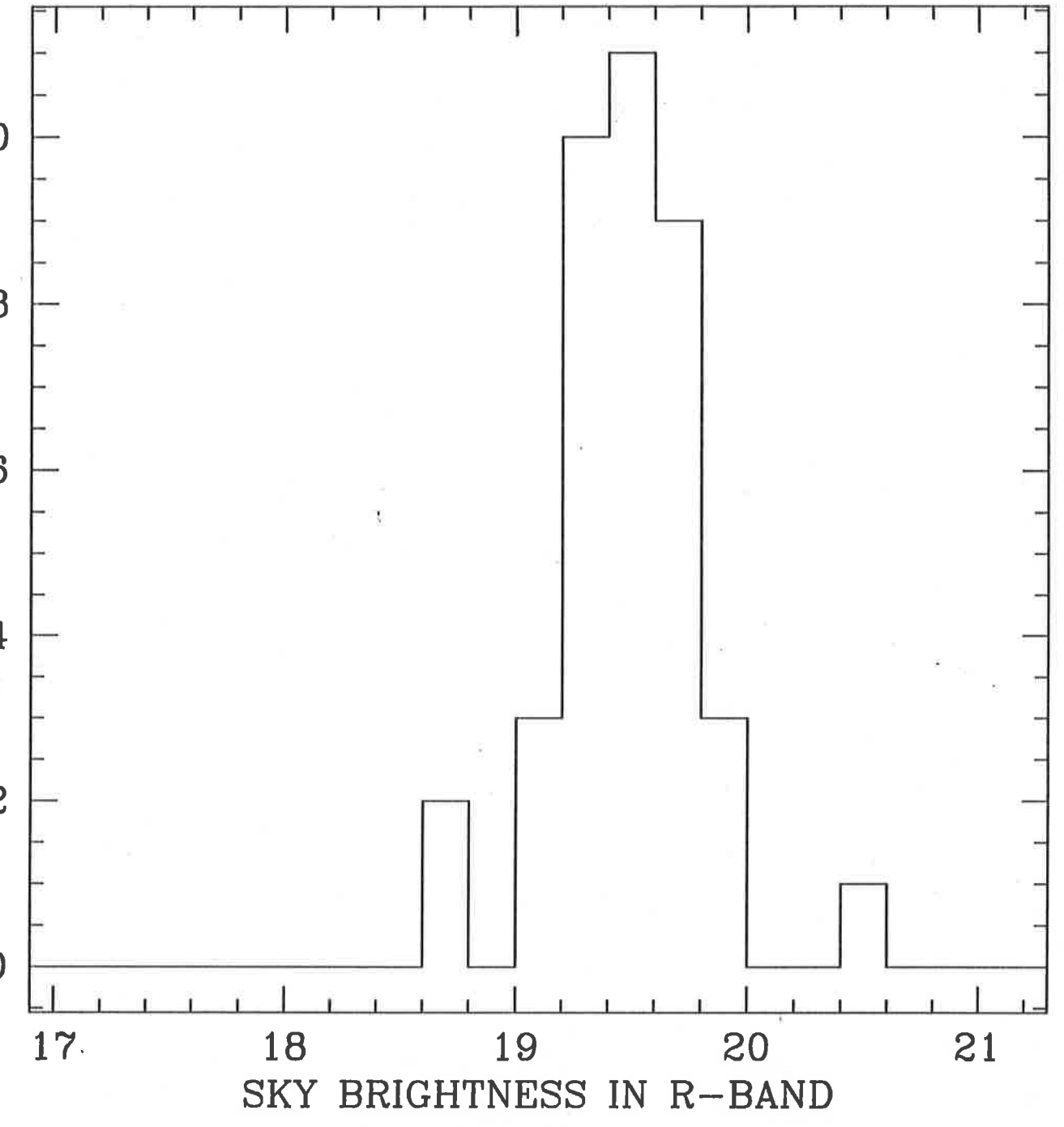

Figure 15. Histogram of the measured sky brightness ($mag/(arcsec)^2$) in R-band during February-May '97.

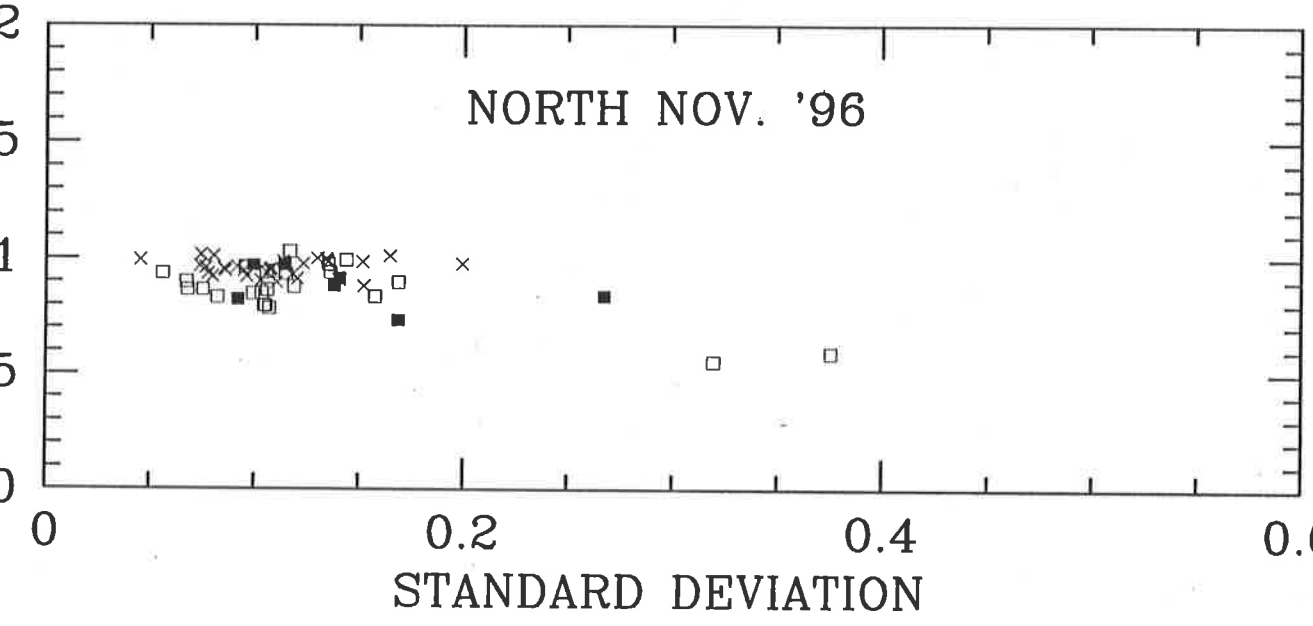
NORTH NOV. '96
0
0.2
0.4
STANDARD DEVIATION

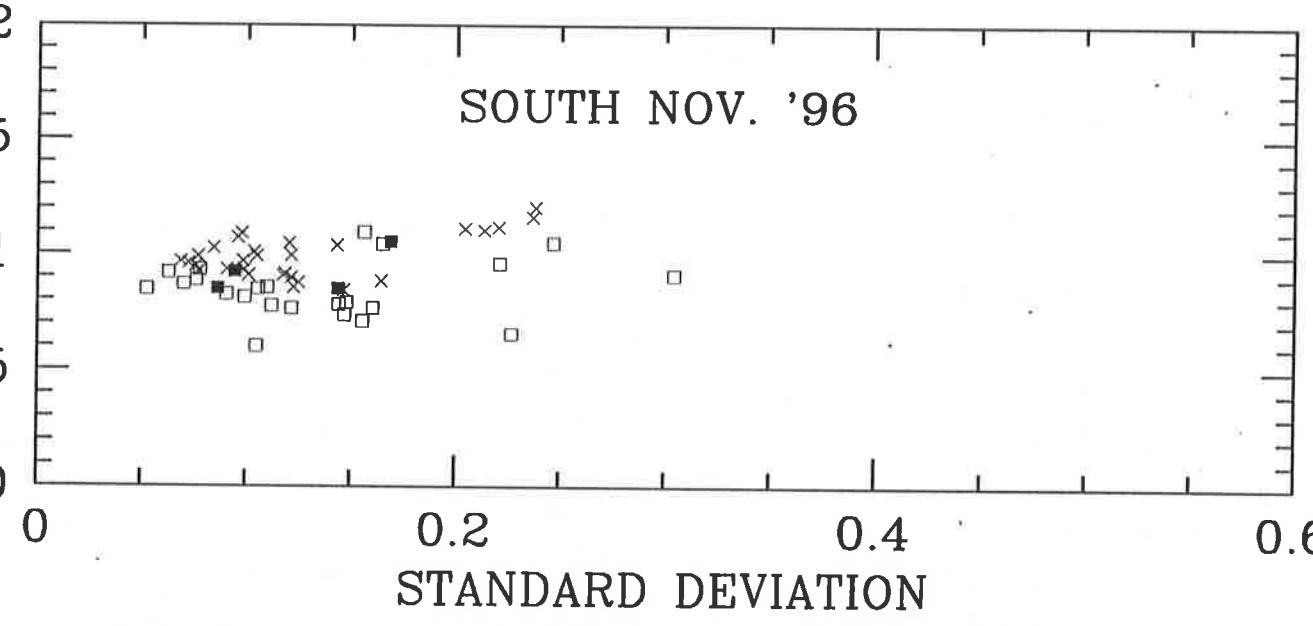
SOUTH NOV. '96
0
0.2
0.4
STANDARD DEVIATION

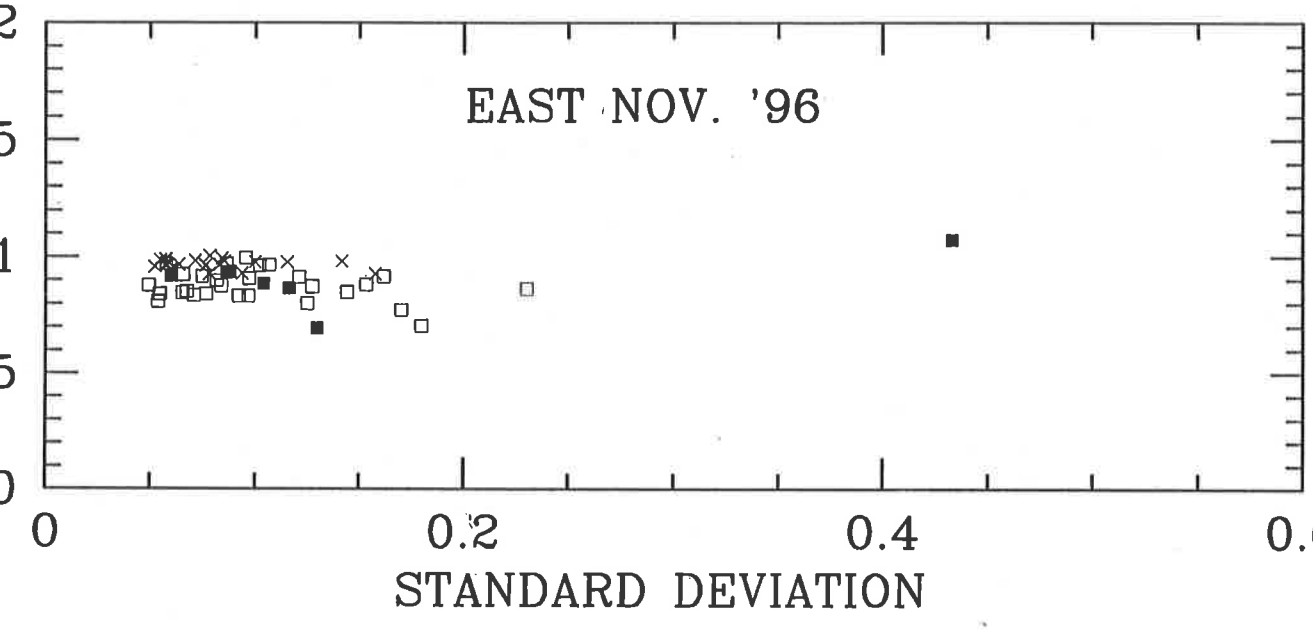
EAST NOV. '96
0
0.2
0.4
STANDARD DEVIATION

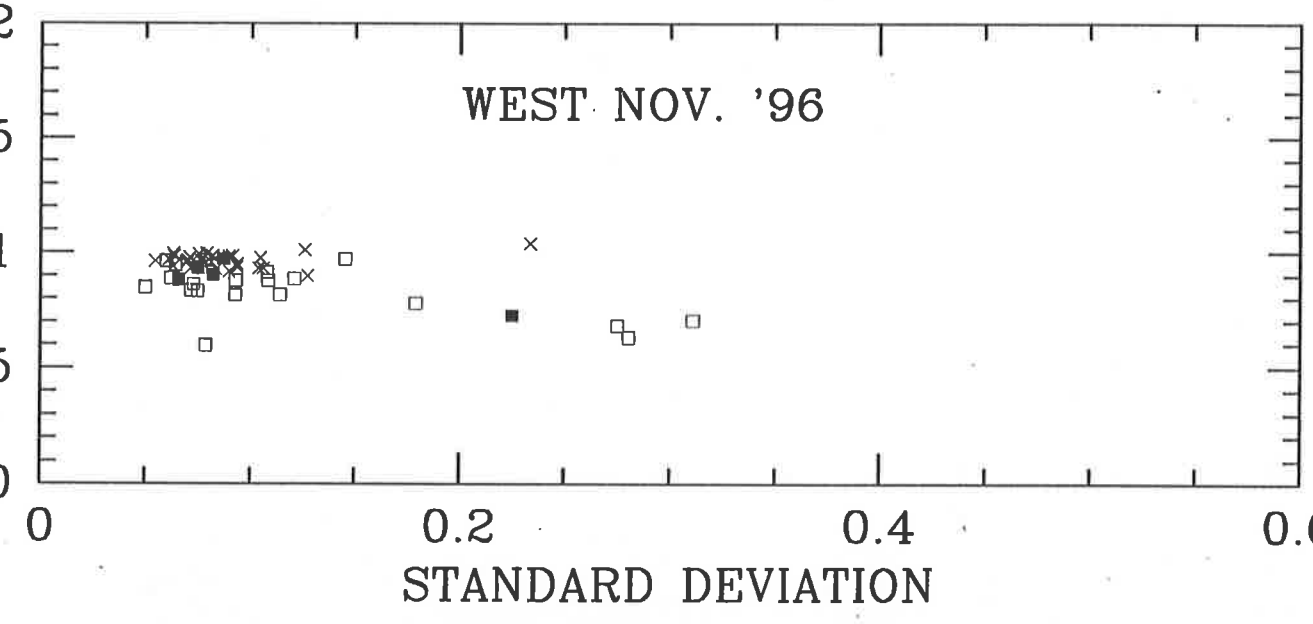
WEST NOV. '96
0
0.2
0.4
STANDARD DEVIATION

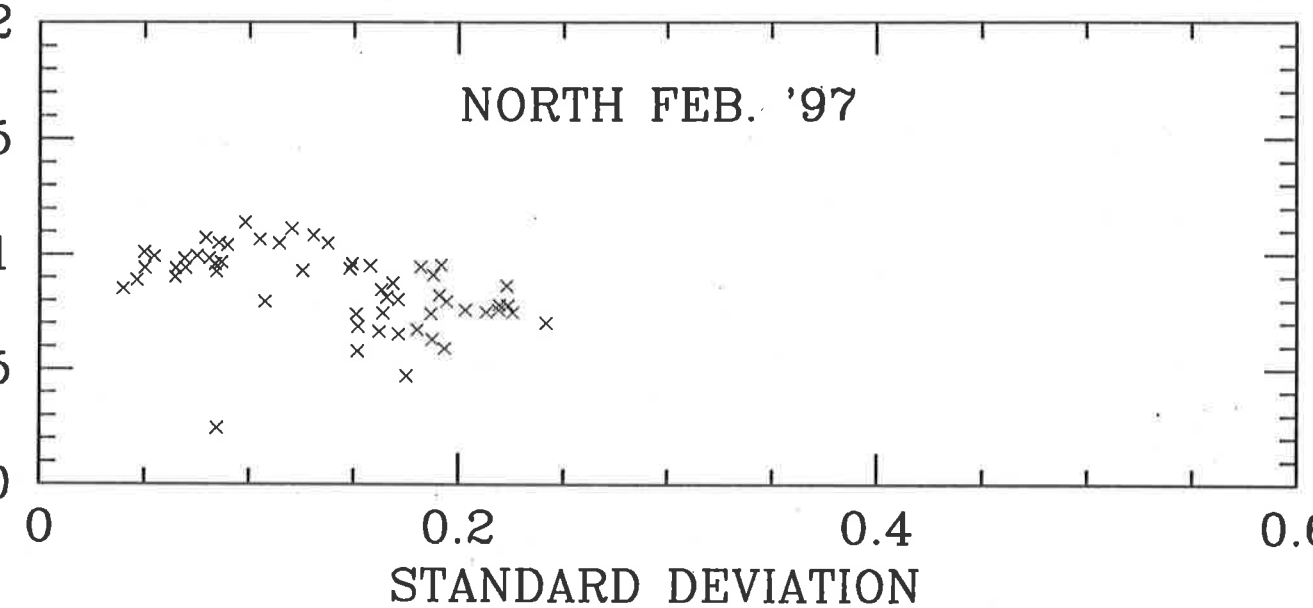
NORTH FEB. '97
0
0.2
0.4
STANDARD DEVIATION

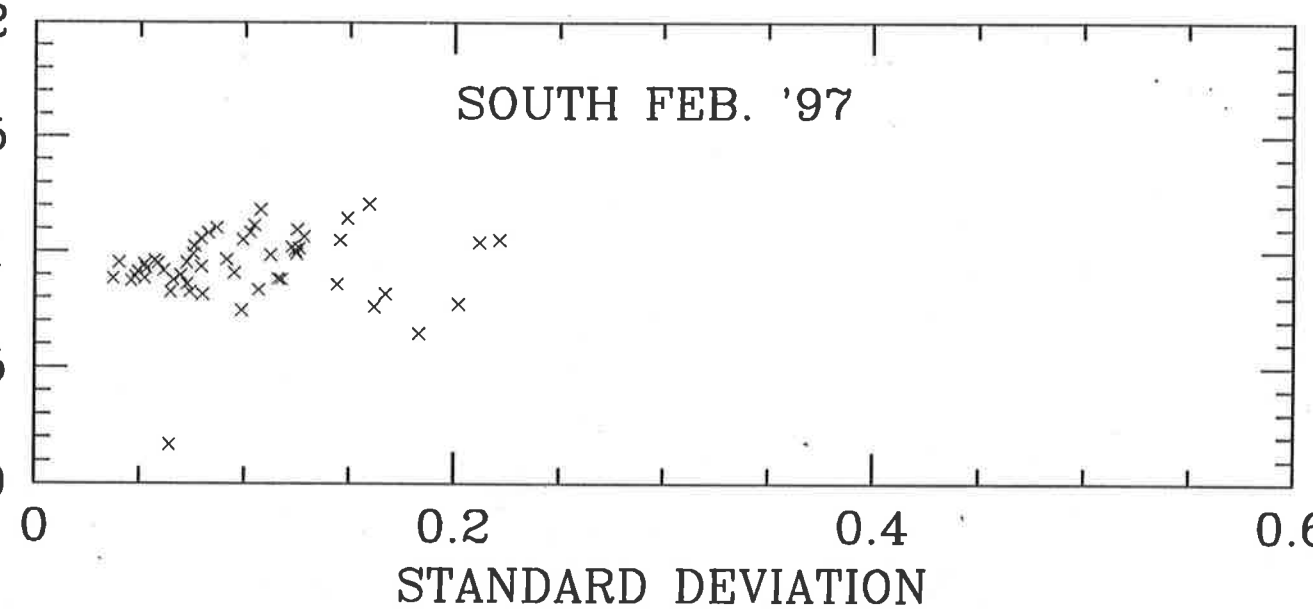
SOUTH FEB. '97
0
0.2
0.4
STANDARD DEVIATION

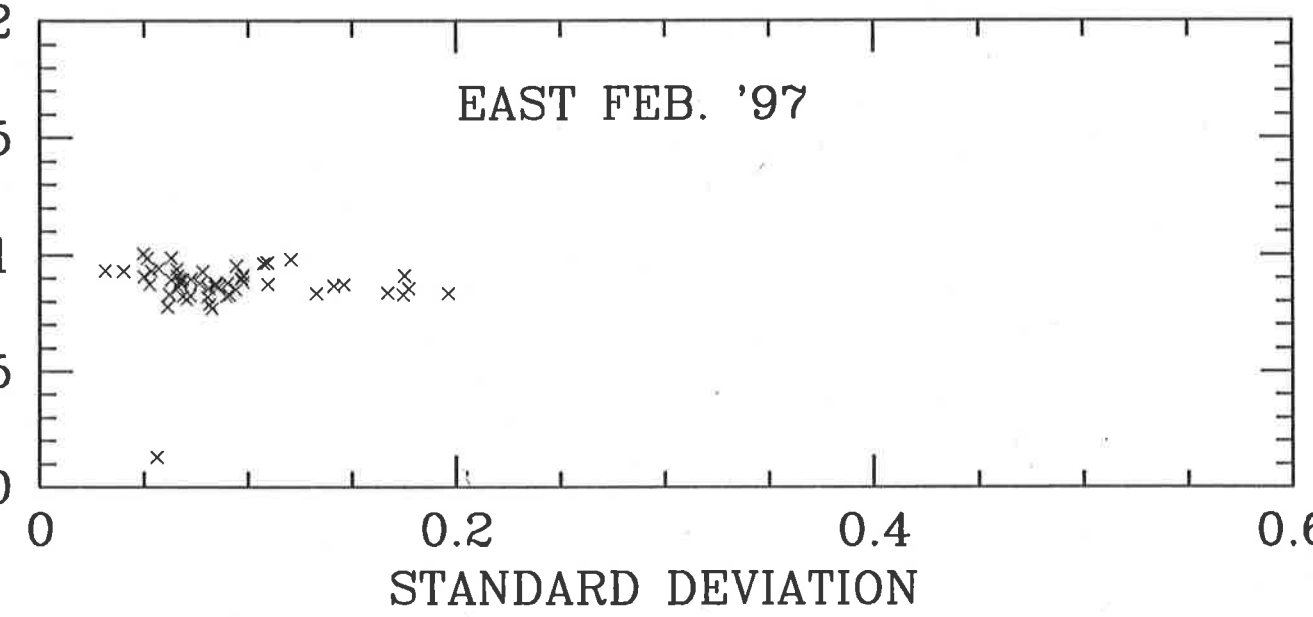

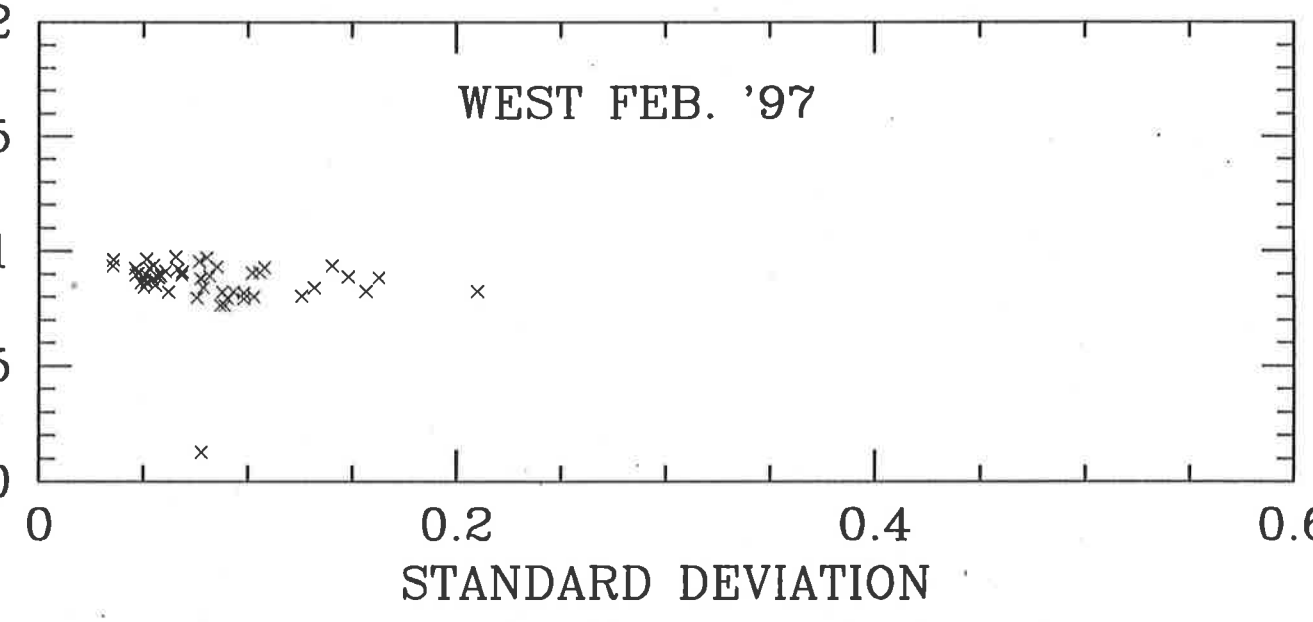

Figure 16. Mean and standard deviation of the flux ratios for star fields corresponding to the different directions are shown for the months of Nov. '96 and Feb. '97 respectively. The cross points stand for nights which are both photometric and spectroscopic, square boxes stand for nights which are only spectroscopic, and the the solid boxes represent nights which have been rejected as per Section-4.1.

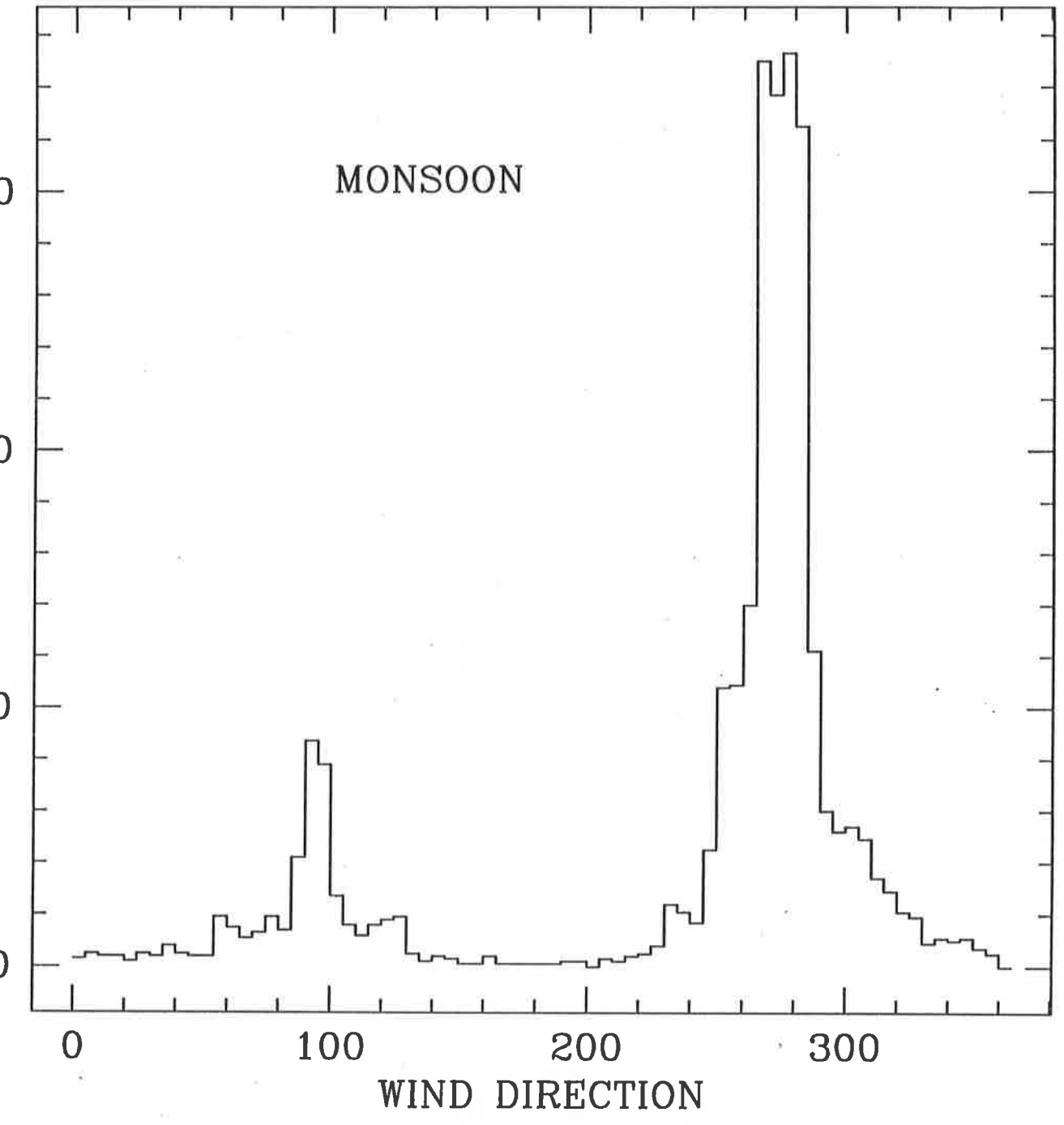

Figure 17. Average wind direction (in degrees, with North, East, South and West corresponding to 0,90,180 and 270 degrees respectively) at night (19:00 hrs. to 05:00 hrs.) during June '96 to October '96.

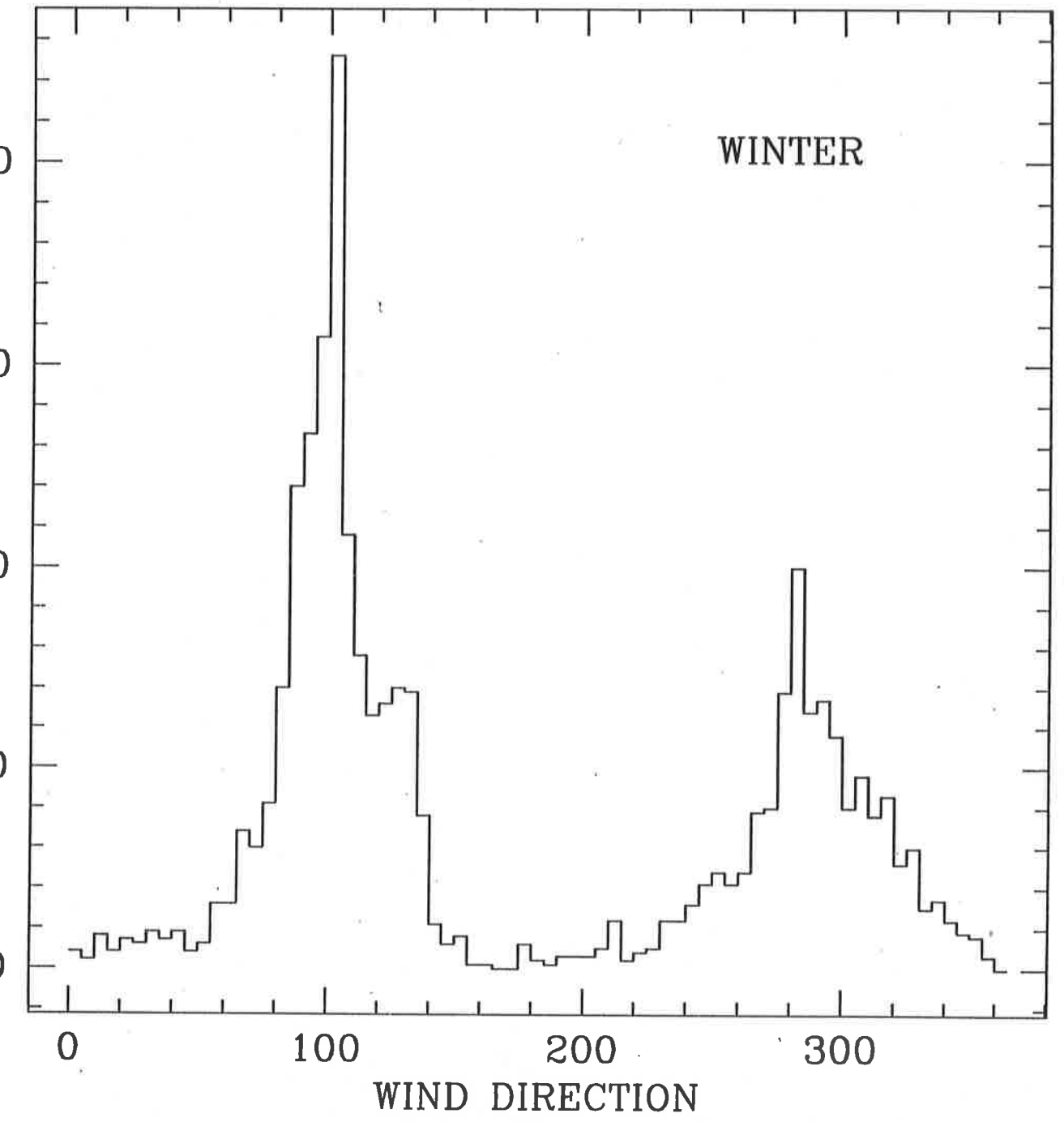

Figure 18. Average wind direction (in degrees, with North, East, South and West corresponding to 0,90,180 and 270 degrees respectively) at night (19:00 hrs. to 05:00 hrs.) during November'96 to February '97.

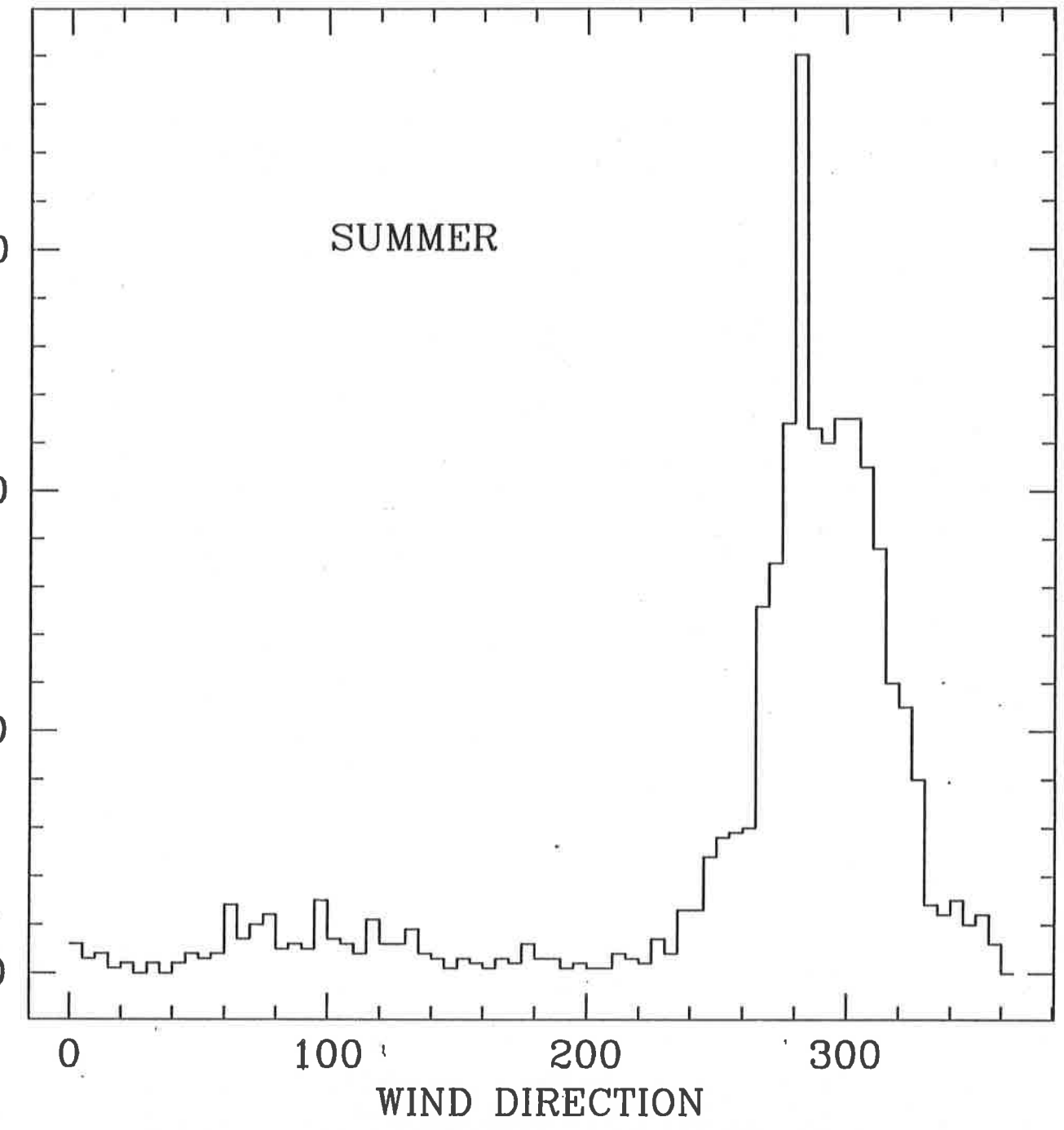

Figure 19. Average wind direction (in degrees, with North, East, South and West corresponding to 0,90,180 and 270 degrees respectively) at night (19:00 hrs. to 05:00 hrs.) during March '97 to May '97.

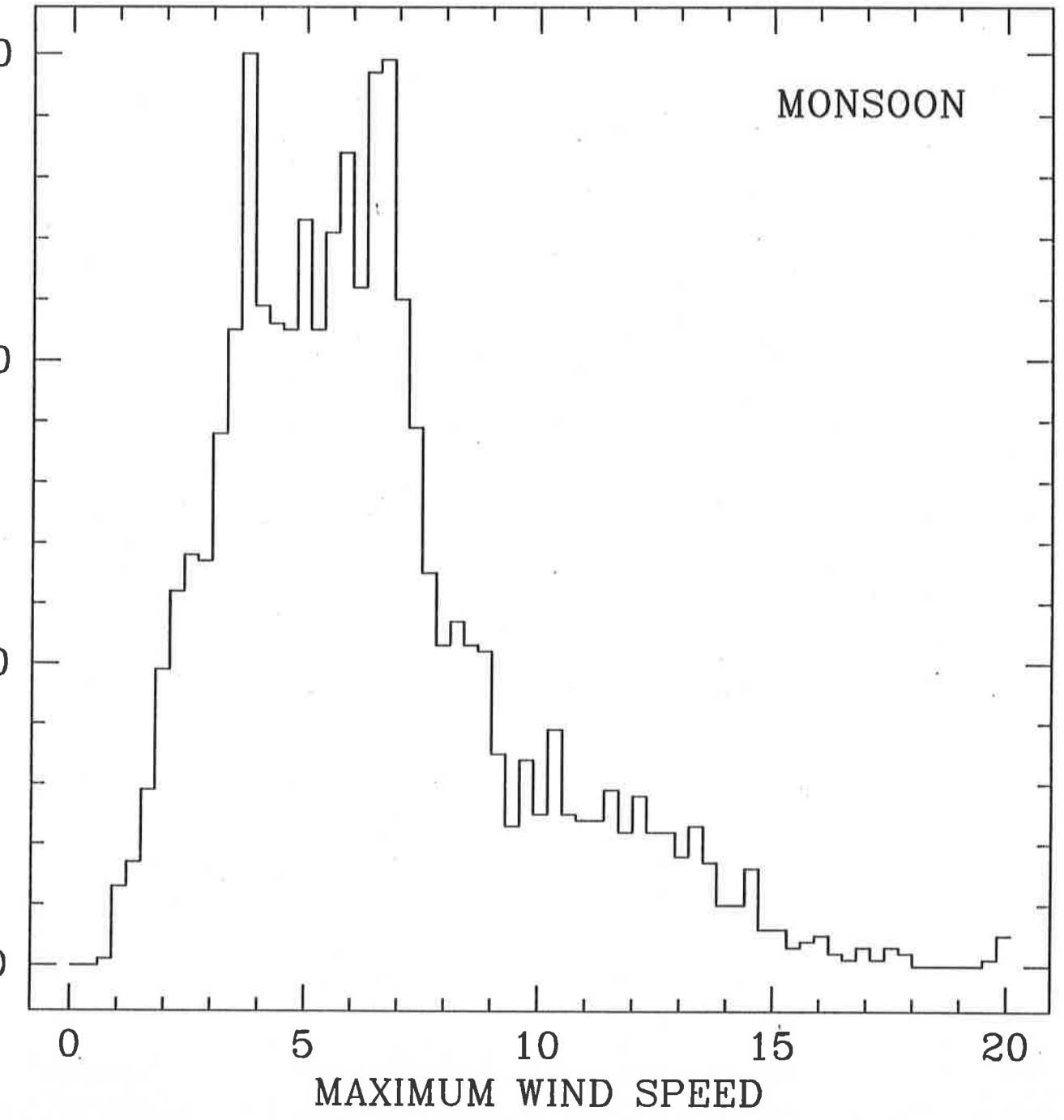

Figure 20. Maximum wind speed (meters/sec) at night (19:00 hrs. to 05:00 hrs.) during June '96 to October '96.

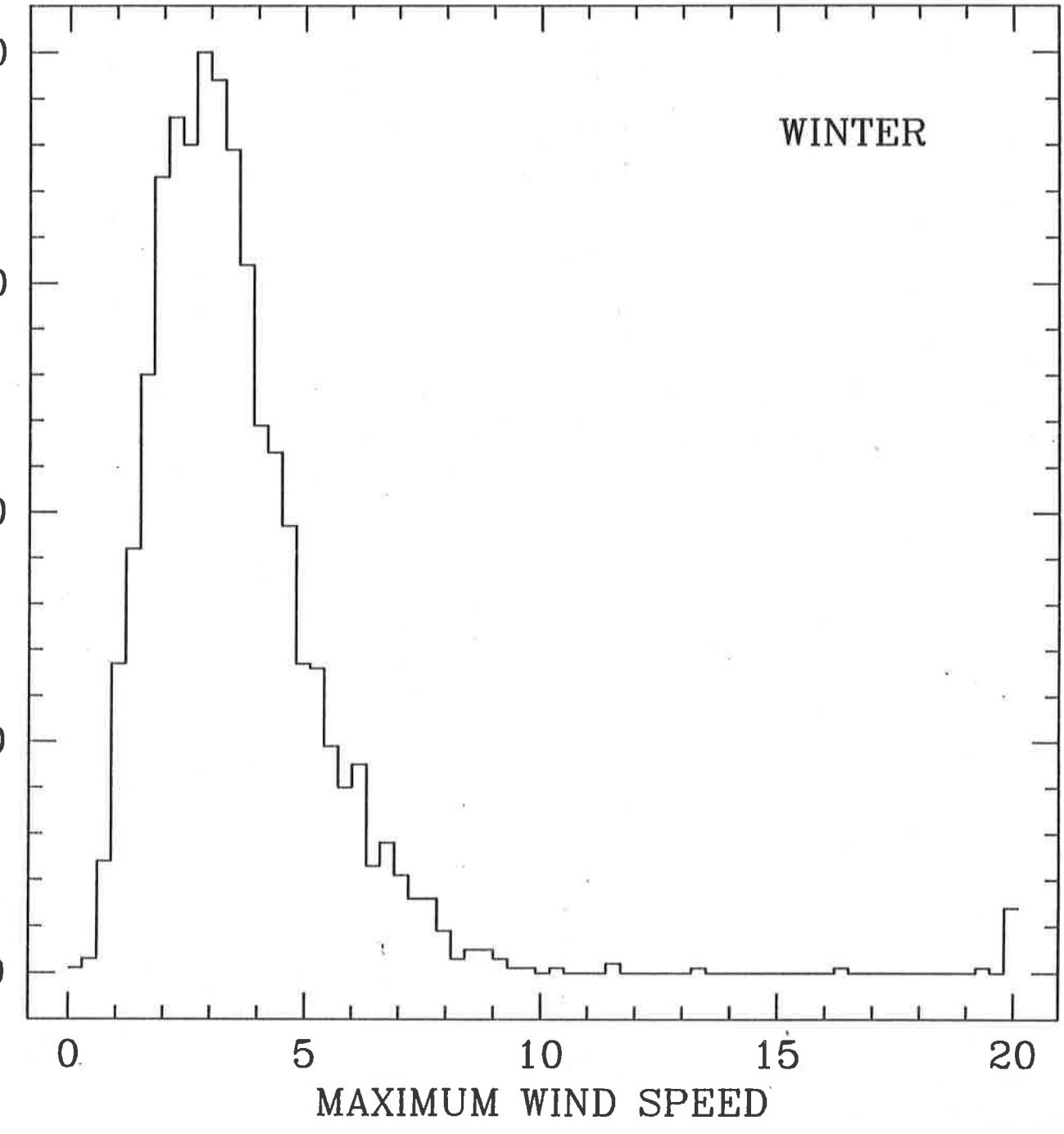

Figure 21. Maximum wind speed (meters/sec) at night (19:00 hrs. to 05:00 hrs.) during November'96 to February '97.

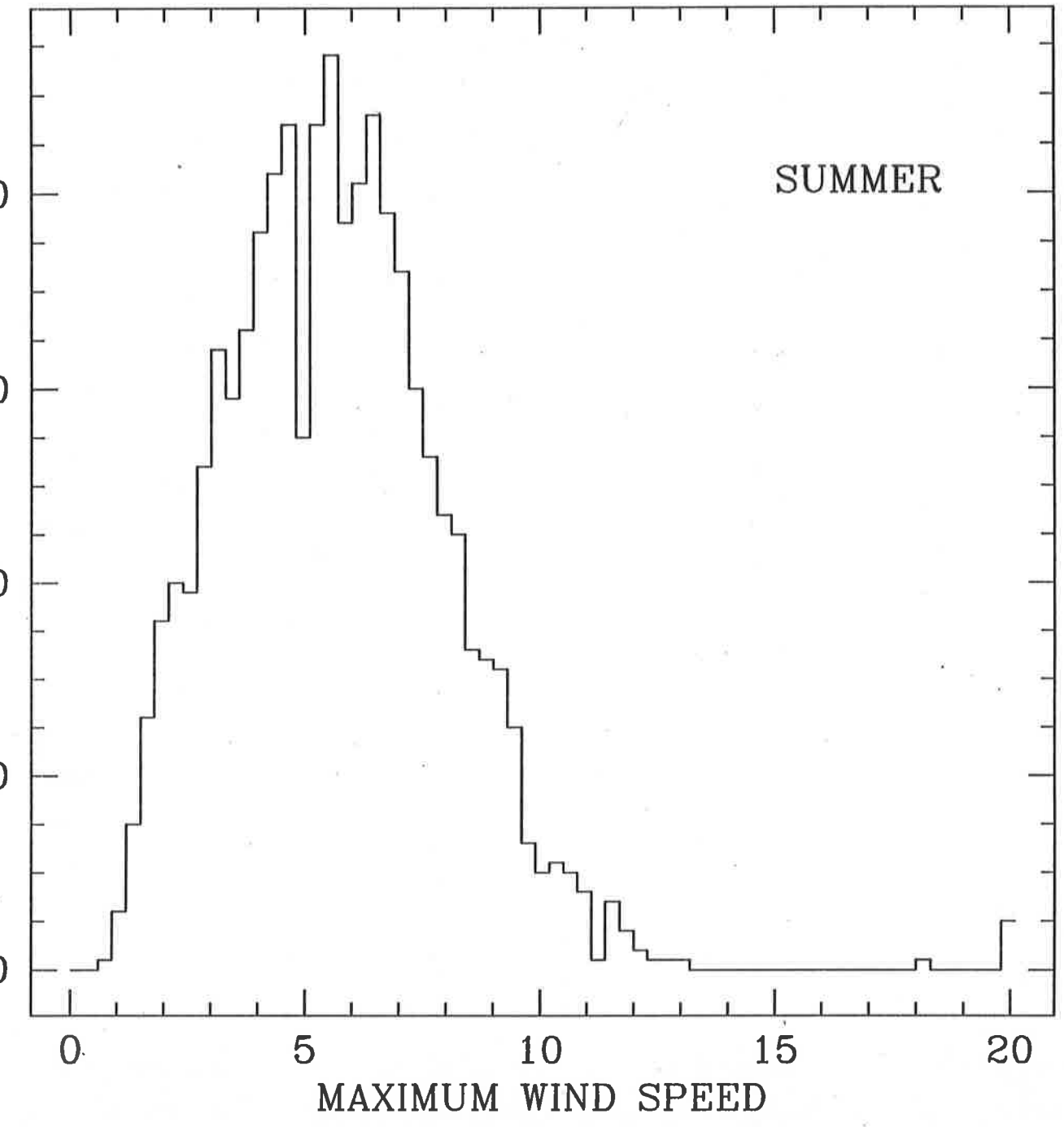

Figure 22. Maximum wind speed (meters/sec) at night (19:00 hrs. to 05:00 hrs.) during March '97 to May '97.

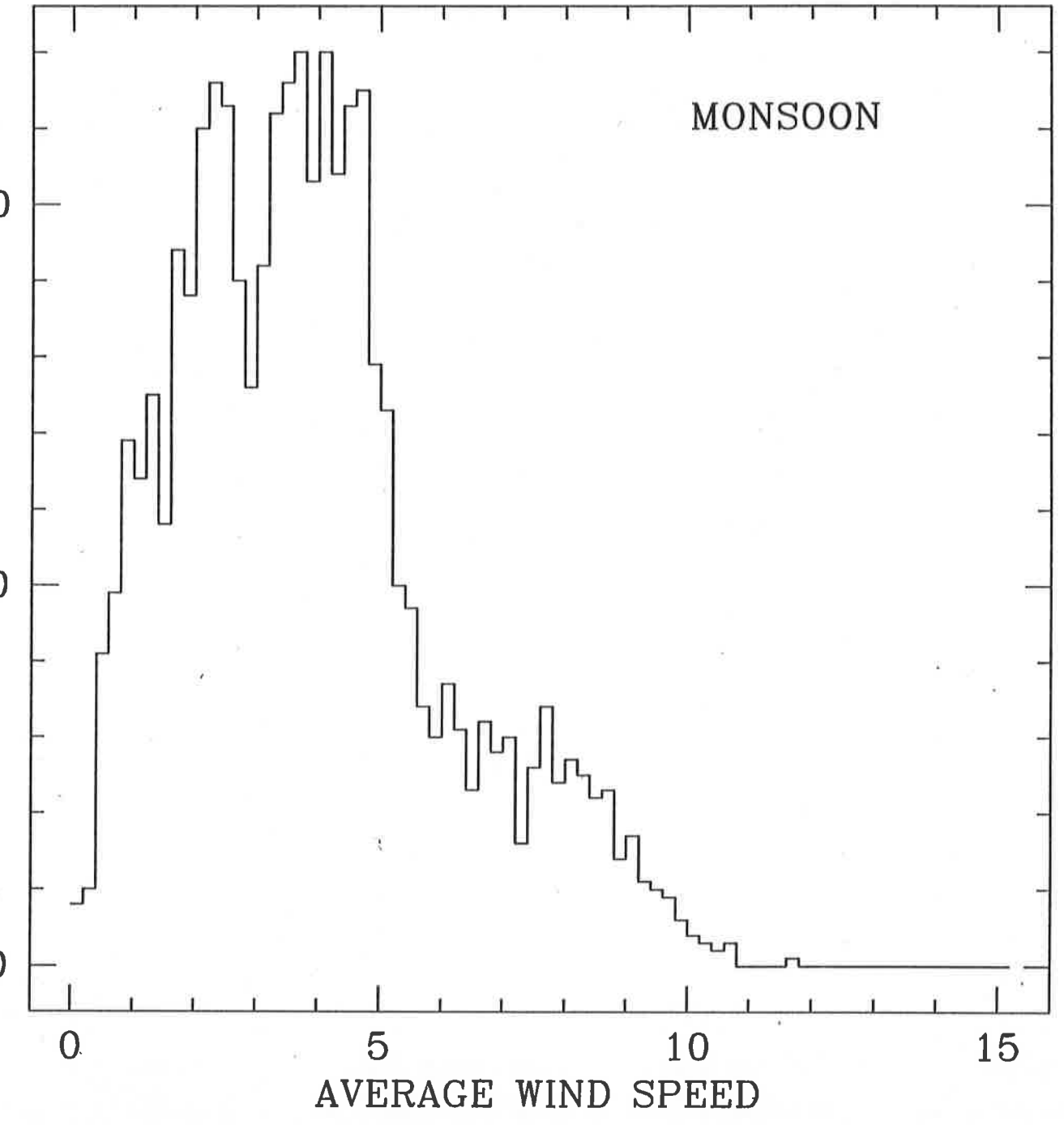

Figure 23. Average wind speed (meters/sec) at night (19:00 hrs. to 05:00 hrs.) during June '96 to October '96.

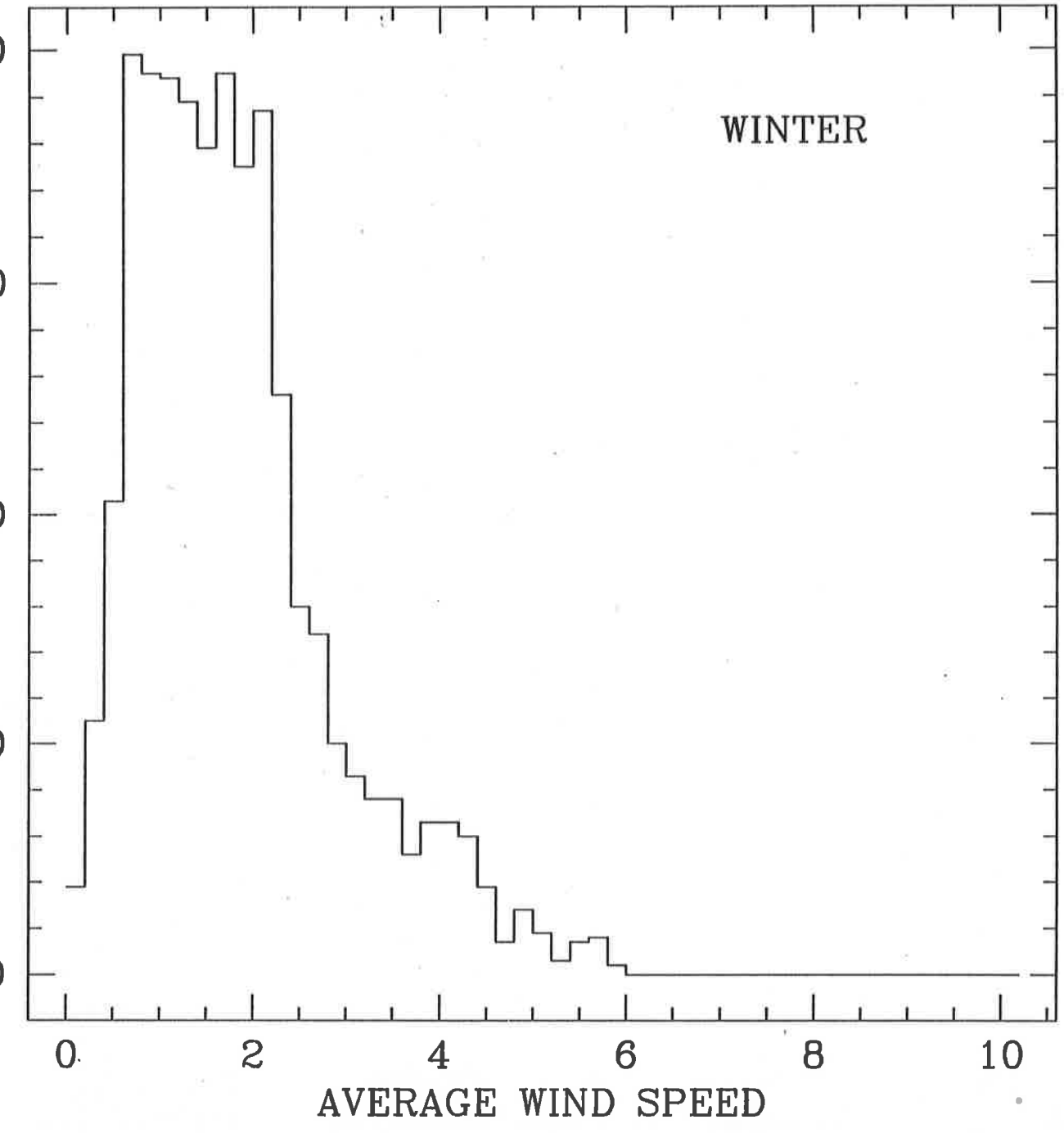

Figure 24. Average wind speed (meters/sec) at night (19:00 hrs. to 05:00 hrs.) during November'96 to February '97.

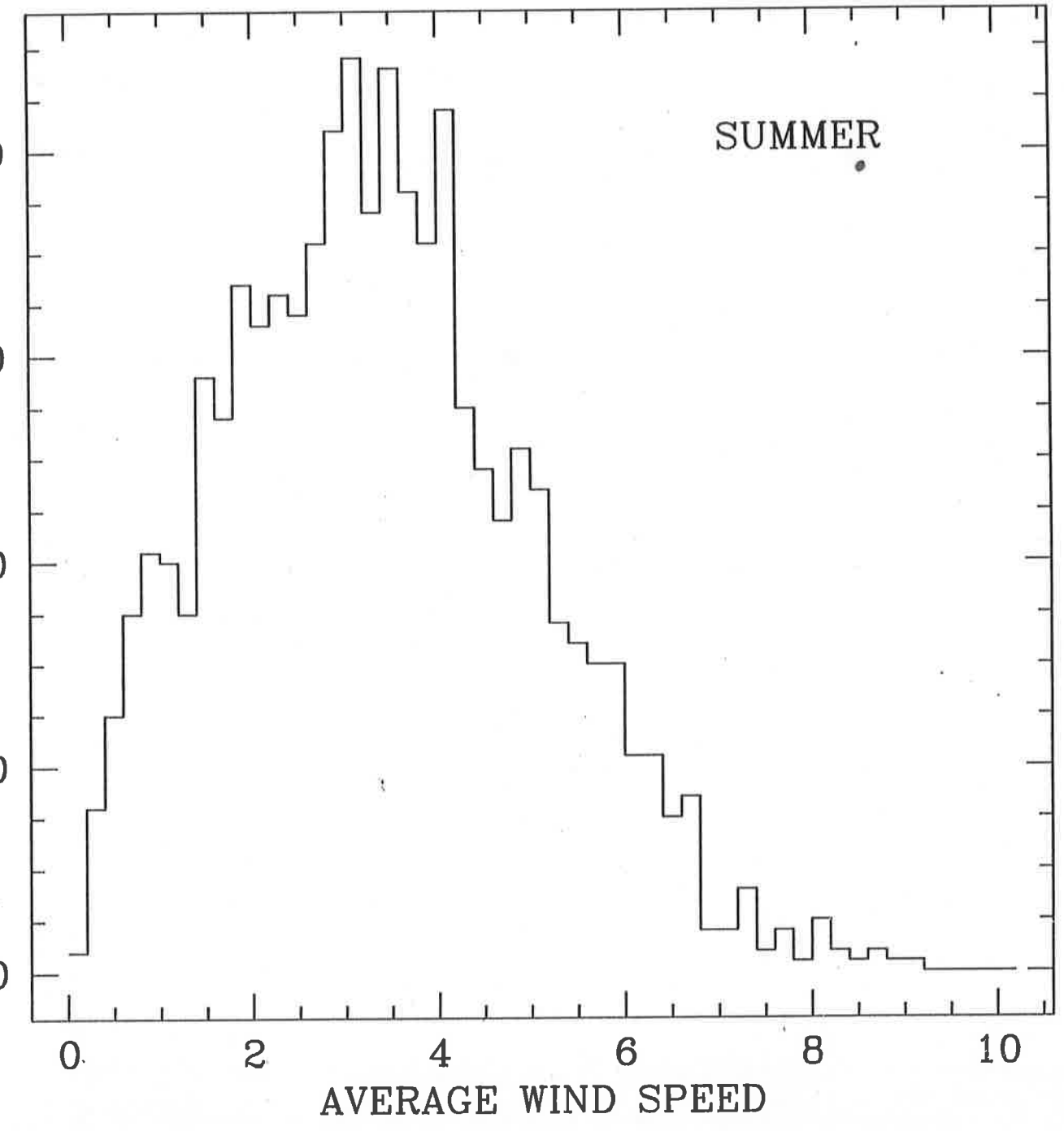

Figure 25. Average wind speed (meters/sec) at night (19:00 hrs. to 05:00 hrs.) during March '97 to May '97.